AD NUMBER

AD871900

NEW LIMITATION CHANGE

TO

Approved for public release, distribution unlimited

FROM

Distribution authorized to DoD only; Administrative/Operational Use; APR 1970. Other requests shall be referred to Air Force Avionics Lab., Wright-Patterson AFB, OH 45433.

AUTHORITY

AFAPL ltr, 25 May 1973

AD871900

DEVELOPMENT OF A FLEXIBLE ABLATOR FOR EXPANDABLE RE-ENTRY BODIES

A. L. LEVINE

R. C. THUSS

D. E. FLORENCE, ET AL

General Electric Company

TECHNICAL REPORT AFAPL-TR-70-15

APRIL 1970

AIR FORCE AVIONICS LABORATORY
AIR FORCE SYSTEMS COMMAND
WRIGHT-PATTERSON AIR FORCE BASE, OHIO 45433

NOTICE

When Government drawings, specifications, or other data are used for any purpose other than in connection with a definitely related Government procurement operation, the United States Government thereby incurs no responsibility nor any obligation whatsoever; and the fact that the government may have formulated, furnished, or in any way supplied the said drawings, specifications, or other data, is not to be regarded by implication or otherwise as in any manner licensing the holder or any other person or corporation, or conveying any rights or permission to manufacture, use, or sell any patented invention that may in any way be related thereto.

AFAPL-TR-70-15

DEVELOPMENT OF A FLEXIBLE ABLATOR FOR EXPANDABLE RE-ENTRY BODIES

A. L. LEVINE

R. C. THUSS

D. E. FLORENCE, ET AL

This report was prepared by the Re-Entry and Environmental Systems Division of the General Electrical Company under USAF contract number F33615-69-C-1713 project number 8170, project task 817004. The work was administered under the direction of project engineer Robert P. Huie for the Air Force Aero Propulsion Laboratory. This report was submitted for approval of the contracting agency on September 30, 1969.

This technical report has been reviewed and is approved:

APPROVED:

F. W. Forbes
Chief, Technical Activities
Operations Office
Air Force Aero Propulsion
    Laboratory

ABSTRACT

Candidate materials suitable for use in thermal shield systems on foldable structures have been evaluated. Thermal shield folding techniques compatible with both the mechanical truss and Airmat ENCAP structures also were defined.

Environmental requirements have been invest'gated for various orbital conditions, and entry conditions have been defined for a range of orbits compatible with the ENCAP missions.

All materials under consideration in Phase I have been determined to be thermally adequate for the required missions.

A foldability rating index has been established on the basis of material mechanical properties. This index has been used as the basis for the material tradeoffs and selection of the prime thermal shield system.

The thermal shield system selected for further study is a composite elastomer'c shield material consisting of a GE Blue overlay on ESM 1030.

This contract was terminated at the convenience of the contracting agency immediately after the initiation of the Phase II effort.

CONTENTS

ILLUSTRATIONS

1. INTRODUCTION

This contract was oriented towards the development of a flexible ablator, compatible with mechanical truss and Airmat structures developed under the ENCAP program. This final technical report covers General Electric Company, Re-entry and Environmental Systems Division (GE/RESD) effort prior to termination of the program. During this period orbital and re-entry environments have been defined, candidate material properties established, and thermal shield folding techniques compatible with the required structures have been investigated and defined.

1.1 MATERIAL SYSTEMS

Candidate materials, Table 1, were selected for preliminary analysis on the basis of their projected capability to meet the general mission requirements, combined with their adaptability to efficient folding, storage and deployment as a part of the ENCAP vehicles. These materials fall into the class of low density elastomers which combine high ablation performance with flexibility.

TABLE 1. CANDIDATE MATERIALS

Material	Description	Density (Lb/Ft^3)
*G. E. Blue	Inorganic Fiber, or Cloth Reinforced Vinyl Silicone	80
TBS-757	Chemically Foamed, Commercial Vinyl Silicone	43
**ESM 1040 (experimental)	Chemically Foamed, Inorganic Fiber, Reinforced, Vinyl Silicone	25-50
NASA-602	Methyl Silicone, Syntactic Foam	35
*ESM 1004-XH	Chemically Foamed, Methylphenyl Silicone, Inorganic Fiber Reinforced	23
*ESM-1030-1	Chemically Foamed, Modified Epoxy-silicone	18
*ESM-1004-X	Reduced pressure Foamed ESM 1004-XH	15

*GE/RESD Proprietary Material
**Old Designation for Flexible Silicone Ablator Series 1040, FSA-1040

2. THERMODYNAMICS

2.1 ORBITAL ENVIRONMENT

The external thermal environment of an orbiting vehicle consists of radiant energy from the sun, solar radiation reflected by the earth or clouds (albedo) and radiation emitted directly by the earth. An orbital altitude consistent with an orbital lifetime of several revolutions must be at least 90 nautical miles. Aerodynamic heating effects above this altitude are negligible. The vehicle and mission characteristics that contribute to the temperature response of a vehicle surface include:

1) Optical properties of the surface or surface coating which includes solar absorbtivity, α, and infrared emissivity, ϵ

2) Angle, β, measured between the earth-sun line and the orbital plane

3) Vehicle orientation with respect to earth, i.e., controlled or uncontrolled

4) Thermal characteristics of the shield-structure composite, i.e., thermal conductivity (k), density (p), specific heat (C_p)

5) Heat available from the vehicle interior due to electrical component dissipation or the heat capacity of payload

2.2 ORBITAL TEMPERATURE RESPONSE

For specific combinations of the above parameters, an equilibrium cycle of temperature response is eventually obtained. The time required to arrive at an equilibrium cycle of temperature response is dependent, of course, on the precise combinations of the above parameters and may occur during the first orbit of exposure or some subsequent orbit. For $\beta = 90^\circ$, and no vehicle roll motion, one side of the vehicle is continuously exposed to solar radiation and the other side is viewing black space. This condition sets up a steady state circumferential temperature gradient around the vehicle. For $\beta = 0^\circ$, and no vehicle roll motion, the vehicle travels in and out of sunlight and earth shadow, thus setting up a cyclical temperature response that eventually reaches some equilibrium cycle. Random sampling of available flight data, Reference 1, indicates the following temperature swings during one orbital cycle:

Exposed Material Composite	ϵ	Solar β ~ Degrees	Maximum Temperature ~ $^\circ$F	Minimum Temperature ~ $^\circ$F
0.060" Al. with insulated back-face	0.8	0°	+180	-60
0.2" PN over 0.1" PG with insulated back-face	0.8	30-40°	+ 80 on backface of PG	-90

2

Of.course, if the material sample had been continuously shadowed and essentially isolated from the orbiting vehicle, the minimum temperature observed would have been much lower.

2.3 ERECTABLE SHIELD-STRUCTURE COMBINATIONS

A review of the possible ENCAP missions indicated that the 3 foot vehicle could be stored and/or deployed external or internal to the parent spacecraft. Storage and deployment inside the parent spacecraft would lead to a well defined thermal environment whereas storage and deployment external to the parent spacecraft would lead to a much wider possible range of temperature extremes.

2.4 RECOMMENDED APPROACH FOR ENCAP

The recommended storage location is dependent on the degree of shield system foldability as a function of temperature over a range of approximately $-100^{\circ}F$ to $+250^{\circ}F$. This information together with the particular mission application determines whether an active means of shield-structure temperature control is required. Active temperature control could be provided by such means as integral mesh resistance heaters or low pressure hot gas generators ($120^{\circ}F$).

3

2.5 ENTRY CORRIDOR

The various orbits from which the ENCAP vehicle may have to re-enter have been investigated. Both circular and elliptical orbits were considered, with altitudes ranging from 75 to 300 nautical miles. A summary of the velocity and path angle, at a reference altitude of 400,000 ft., resulting from firing the retro-rocket at various locations in the orbit is presented in Figure 1 which presents the relationship between entry velocity and path angle and the orbital parameters at deboost (orbit anomaly, perigee altitude, eccentricity and inclination). The deboost maneuver is analyzed at GE/RESD using the REO (Return from Elliptic Orbit) program. Note that the velocity and path angles shown are inertial values and, thus, do not show the effect of orbital inclination.

The severity of the hypersonic entry environment is dependent only on the vehicle configuration parameters (R_N, θ_c, W/C_DA, and axial station), entry velocity, and path angle. Hence, definition of the entry environment can essentially be uncoupled from the original orbit and the exospheric de-orbit maneuver and referenced only to the V_E - γ_E corridor illustrated in Figure 1.

2.6 ENTRY ENVIRONMENT

The primary heating parameters which determine shield thickness requirements for a particular ablator are peak heat flux, time-integrated heat flux, and time-width of the heat pulse. Over the broad spectrum of entry conditions, these heating environment parameters can be shown as a function of entry velocity, path angle, and ballistic coefficient as presented in Figure 2. The values shown were developed through the use of the CREWS trajectory program (Reference 2). The CREWS approximate heating equation for the stagnation point is $\dot{q}_0 = 3.16 \times 10^{-9} \rho_\infty^{0.5} u_\infty^3 R_N^{-0.5}$, where the time-histories of the free stream velocity and density are influenced by vehicle shape and size and the atmospheric density profile. The CREWS technique is superior to other approximate techniques which are based solely upon initial entry conditions and an idealized atmosphere.

The approximate technique employed to determine the heating environment over a broad spectrum of entry conditions results in less than 10 percent error in heating which, in turn, translates into a much smaller percentage error in the determination of shield thickness. After design trajectories have been selected on the basis of the trends of the approximate results, more precise tools are used to determine shield thickness for those design points. These tools include the Six-Degree-of-Freedom trajectory program and the Planetary Aerodynamic Heating Program (PAHP) described in Appendix A.

Figure 2 shows peak cold wall convective heat flux, time-integrated convective heat flux, and time-width of the heat pulse as a function of path angle and ballistic coefficient, for a 3 foot base diameter, 50° sphere cone with a bluntness ratio of 0.6, and an initial
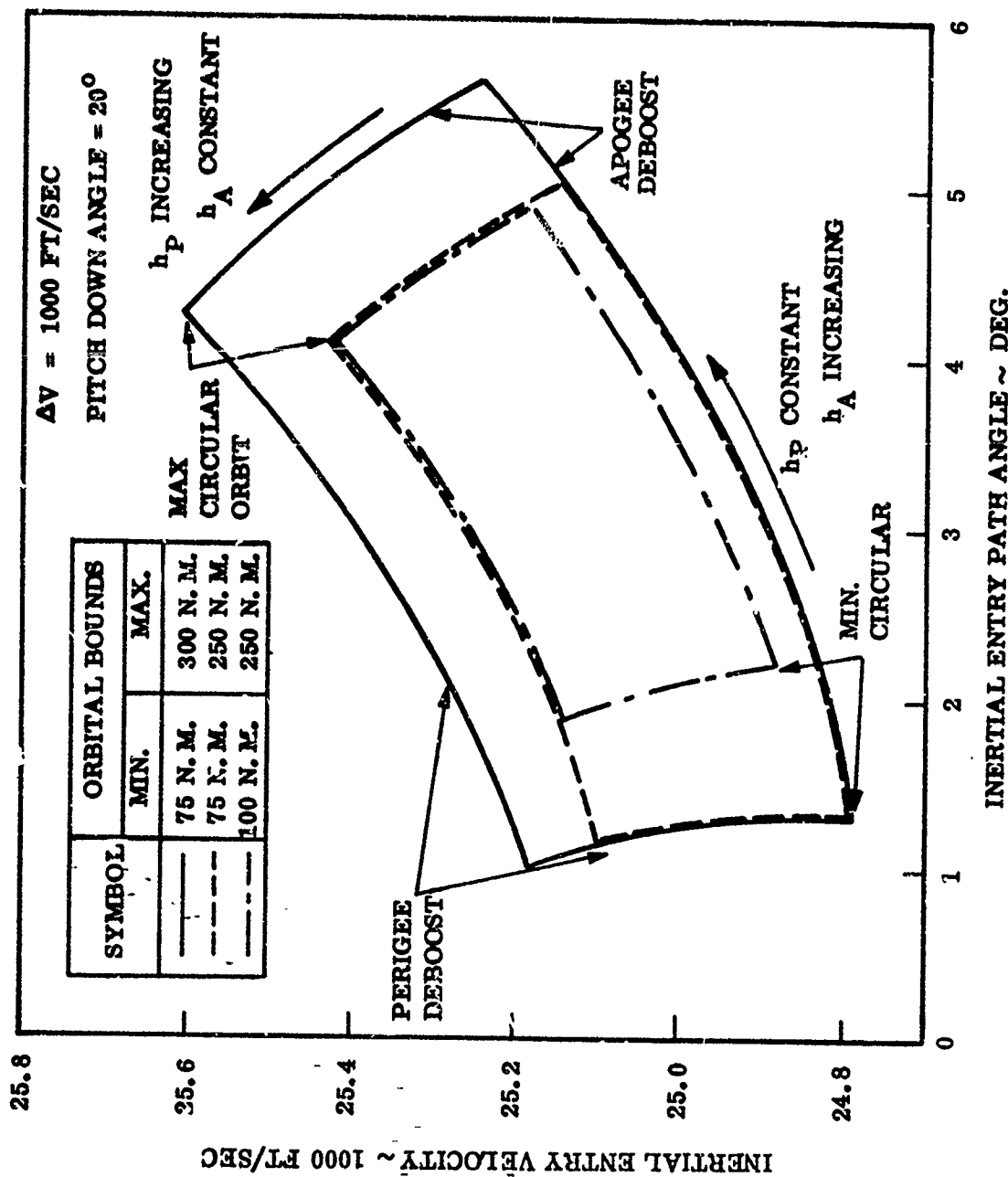
4

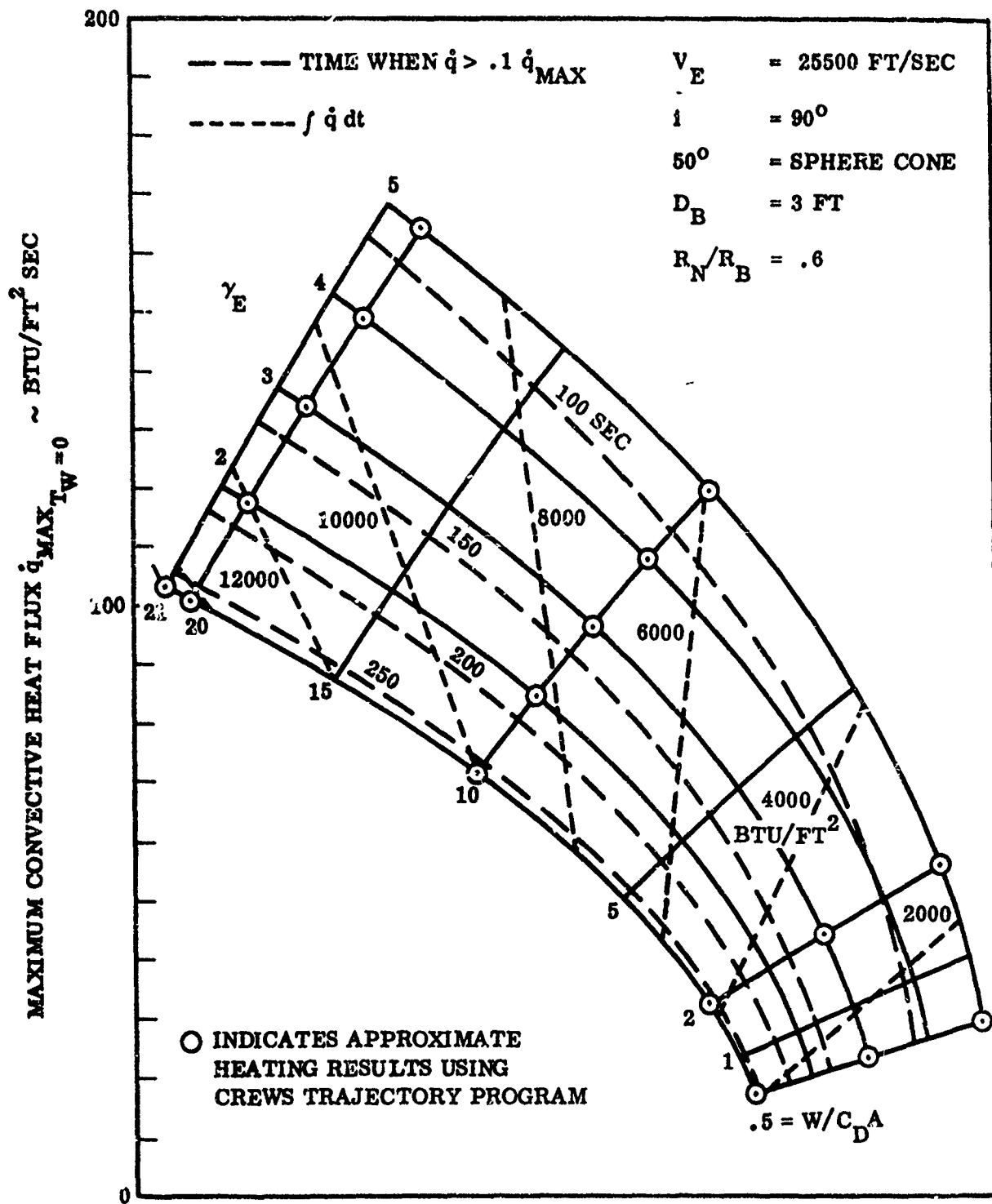Figure 1. V – γ at 400,000 FT

Figure 2. Effect of Ballistic Coefficient and Initial Path Angle on Entry Heating Environment

6

entry velocity of 25,500 ft/sec. Heating for the entry corridor defined in Figure 1 is relatively insensitive to entry velocity. The use of a specific entry velocity of 25,500 ft/sec, rather than the actual velocities which range from 24,800 to 25,600 ft/sec, produces errors of less than 9 percent in peak convective heat flux and less than 6 percent in time-integrated heat flux for any point in the entry corridor, and considerably smaller errors for those points considered as design trajectories.

2.7 PRELIMINARY DESIGN TRAJECTORIES

The process of determining shield thickness requirements includes the selection of one or more design trajectories. The insulative thickness requirement increases both with the time-integrated heat flux and the time-width heat pulse. It can be seen in Figure 2 that an entry with a ballistic coefficient of 21 and path angle of 1° is the most severe in both these respects.

For the 3 foot vehicle, which has as a ballistic coefficient of 21, Figure 3 shows the approximate values of the heating parameters as a function of path angle and vehicle station. Depending upon the entry corridor and the shield material used, maximum shield thickness requirements may occur for a steeper trajectory because of recession of the surface of the shield during the ablation process. However, as will be shown, surface recession is not expected to be a factor in the selection of the design trajectory for these candidate material systems and this range of entry conditions.

For the design trajectory at $W/C_DA = 21$, $\gamma = 1^\circ$, the Planetary Aerodynamic Heating Program (PAHP) was used to determine more precise heating as a function of time. Figure 4 shows the heat pulse at the stagnation point, the sphere-cone tangency point, and end of skirt. The design trajectory used by Lockheed is also shown for comparison; note that the GE/RESD preliminary design trajectory is more severe both with respect to time-integrated heating and the time-width of the heat pulse, and thus it will require a greater shield thickness.

2.8 THERMAL PERFORMANCE OF MATERIALS

Figure 5 shows the criterion used to determine the time of boundary layer transition to turbulent flow. By comparison with Figure 4 it can be seen that the 3 foot vehicle turbulent flow does not occur until the heating is insignificant. Therefore, the laminar heating approximations shown in Figures 2 and 3 for the 3 foot vehicle are not affected by consideration of turbulent flow. Figures 6 and 7 show PAHP predictions of heat flux and aerodynamic shear maximums along the vehicle. Note that aerodynamic shear levels are not significant.

Thickness requirements for three well characterized materials of the silicone elastomer family were determined using the Reaction Kinetics Ablation Program (REKAP), Appendix B, and are presented in Figure 8. The three materials used as representatives of the silicone elastomer family were ESM 1004X ($\rho_v = 15$ lbs/ft^3), ESM 1004AP ($\rho_v = 35$ lbs/ft^3), and RTV 560 ($\rho_v = 88$ lbs/ft^3). The REKAP models developed for prediction of thermal response of these materials have been confirmed by several plasma jet ground

7
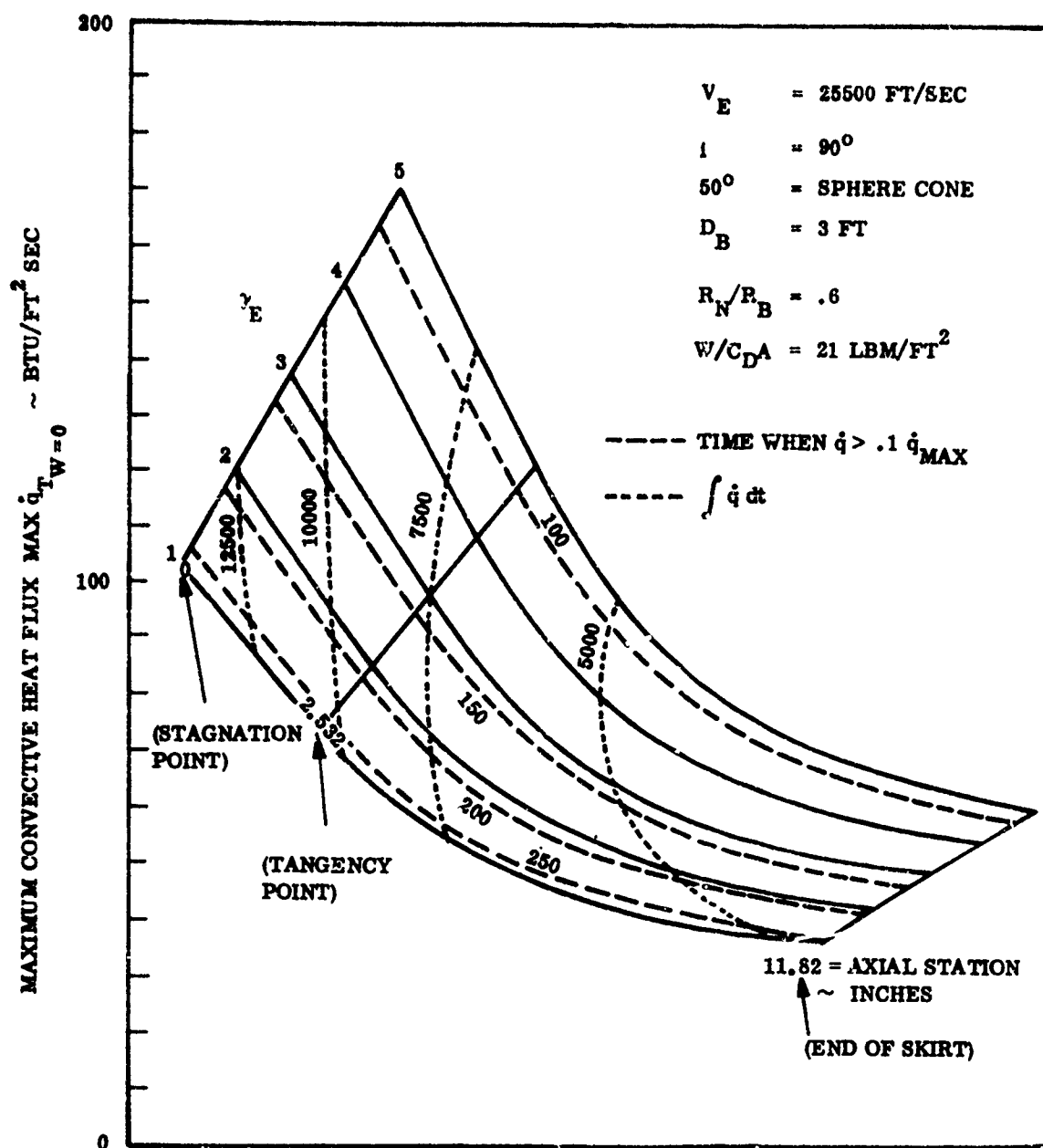
Figure 3. Effect of Vehicle Axial Location and Initial Path Angle on Entry Heating Environment
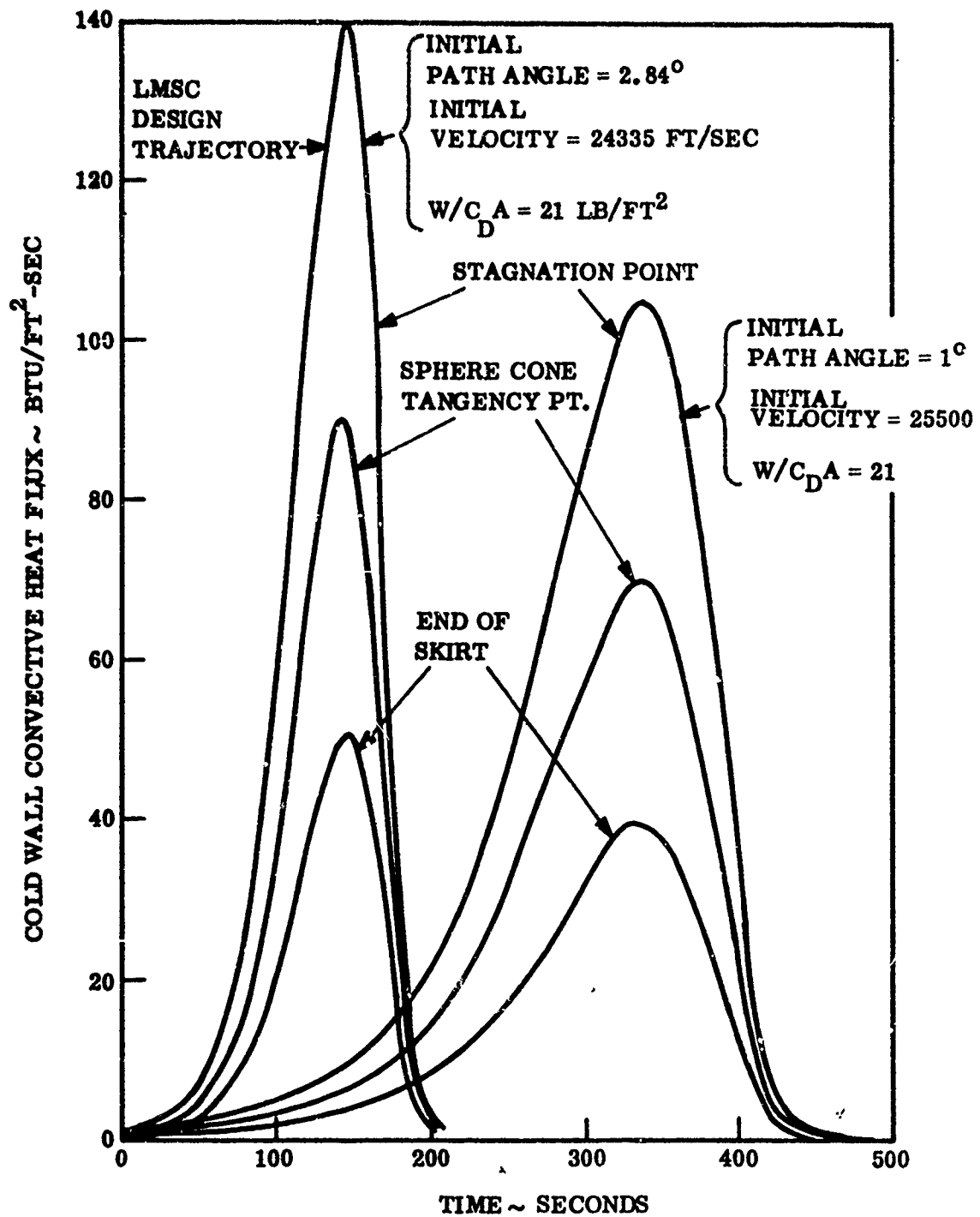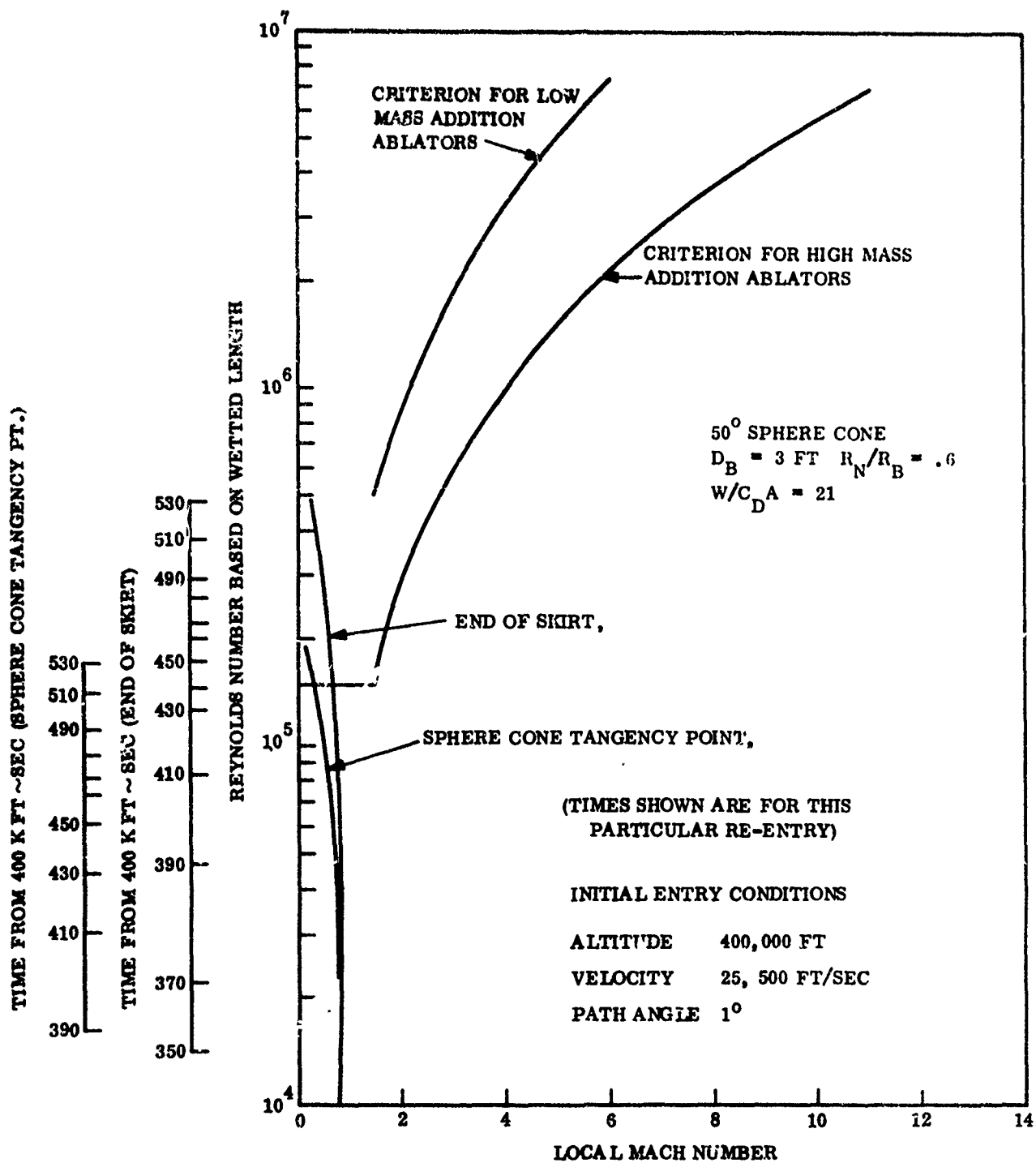
Figure 4. Cold Wall Convective Heat Flux Histories

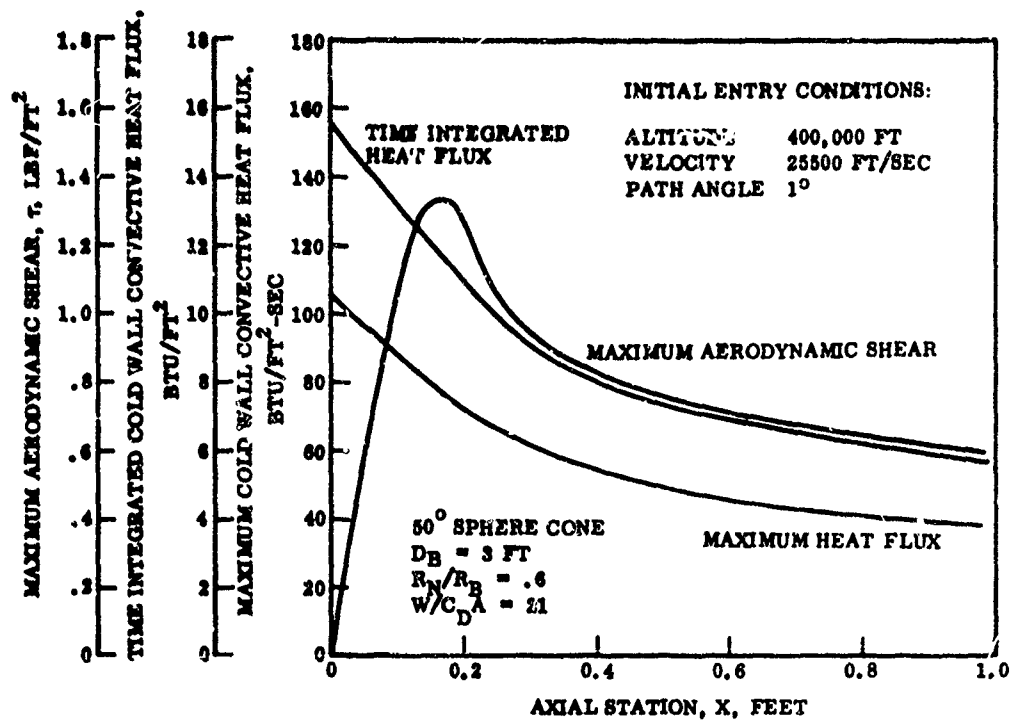Figure 5. Determination of Time of Boundary Layer Transition to Turbulent Flow

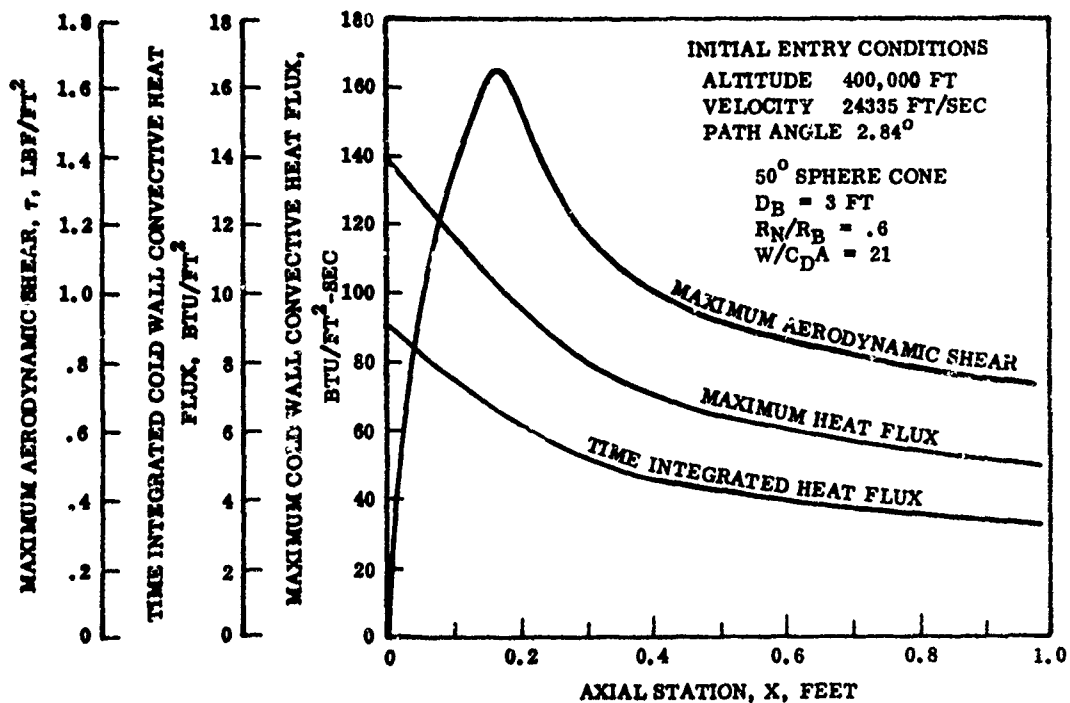**Figure 6. Heating and Maximum Aerodynamic Shear Along the Vehicle**

Figure 7. Heating and Maximum Aerodynamic Shear Along the Vehicle

11

tests both for substrate temperature response and surface recession rates. Reference 3 contains an example of such a development. Surface recession rates of closed cell ESM's of various dens   have been correlated as a function of heat flux, enthalpy, surface pressure, and d   ty of the material. The correlation is presented in Reference 4 and includes da   eight test facilities. Thermophysical properties employed in REKAP are shown in Table 2.

The thicknesses shown in Figure 8 are those required on the stagnation point to prevent the backface temperature from exceeding a given maximum. Note that the relative ranking remains similar across the temperature range. It should also be noted that for the ESM 1004X thicknesses shown it is assumed that a thin layer of high density material is overlayed to prevent direct boundary layer heating in-depth, due to the high surface porosity of this material. If ESM 1004X were used without the overlay, a greater thickness would be required. Throughout this study, a high density overlay is presumed present on all materials where surface porosity would cause increased in-depth heating.

The materials under consideration are all members of the silicone elastomer family and are assumed to have similar internal chemistry. Therefore, the assumption is made that the relative thicknesses required for these materials to protect to a given backface temperature can be assessed by ranking their relative insulative performance. Classical transient temperature response of an insulator of known thickness exposed to a sinusoidal shaped heat pulse of known dimensions is presented by Schneider in Reference 5. From Reference 5, a thermal diffusivity and thickness parameter, α/δ^2, can be determined as a function of $k\rho C_p$, for a given heat pulse; the function approximates a straight line (log scale) over the range of properties and thicknesses evaluated in this study. Figure 9 shows the variation of thermal diffusivity as a function of temperature for the various materials under consideration. It can be seen that the relative properties of each material vary with temperature; thus, in using the present method to compare predicted performances, it is necessary to select a representative temperature to obtain the properties. Figure 10 is adapted from Reference 5. The thicknesses determined by use of the REKAP program are indicated using the proven REKAP material models for three well-characterized materials: ESM 1004X, ESM 1004AP, and RTV 560. The location of the line illustrated as "theory" is that determined by use of Reference 5, using a representative net heat pulse for the entry condition noted. As can be seen, use of material properties at 860°R gave results consistent with theory. Figure 10 can be used, then, to approximate the relative thickness requirements of the other materials. Using this method, based on the properties at 860°R, relative thicknesses have been determined which are presented in Figure 11a (thicknesses are expressed relative to the thickness requirement for ESM 1004X with a high density overlay). Figure 11b presents the relative weight requirements for the same materials. Note that those materials most attractive from the point of view of minimizing thickness are generally least attractive where weight is a consideration. Properties used in this analysis are shown in Table 3.

The materials include composite systems consisting of a low density material overlayed by GE Blue. It was originally thought that minimum thickness and/or weight requirements might be obtained by using a high density overlay material to some particular depth, such as the degradation depth, then using a lower density material as the insulative layer. The validity of this suggestion, in this regime of heating, was assessed and

12

TABLE 2. THERMOPHYSICAL PROPERTIES EMPLOYED IN REKAP

		ESM 1004 X	ESM 1004 AP	RTV 560
Virgin Density, $\rho_v \sim$ lb/ft^3		15	36	88
Char Density, $\rho_c \sim$ lb/ft^3		6.65	14.4	35
Surface Emissivity		.8	.8	.8
Pyrolysis Gas Specific Heat, C_{p_g} Btu/lb $^\circ$R		.4	0.384	.384
Order of Reaction		2	2	1
Pre-exponential Factor, $Z \sim$ sec^{-1}		15,000	30,000	6070
Activation Energy, $E \sim$ Btu/lb Mole		47,700	47,500	40,100
Heat of Decomposition H Btu/lb Gas Generated	1335°R	50	50	50
	1460	45	45	45
	1710	1000	1000	1000
	1960	2610	2610	2610
Specific Heat, C_p Btu/lb $^\circ$R	610°R	.32	0.313	.313
	710	.327	0.365	.365
	1210	.440	0.440	.44
	2075	.440	0.440	.44
Conductivity, k Virgin Btu/ft – sec $^\circ$R	610°R	.0000130	.0000237	.0000619
	860	.0000178	.0000219	.0000572
	1335	.0000206	.0000211	.0000551
	1710	.00002349	.0000237	.0000619
Char	1335	.0000670	.0000781	.000204
	1710	.0000765	.0000876	.000229
	2210	.0000902	.0001036	.000270

TABLE 3. PROPERTIES AT 860°R

	$k \times 10^5$	ρ	Cp	$\alpha \times 10^5$	$(k\,\rho\,Cp)^{.5}$
ESM 1004X	1.78	15	.37	.3204	.00993
ESM 1030–1	1.37	18	.477	.1597	.01085
NASA 602	2.06	35	.40	.1472	.0170
TBS 757	2.05	43	.365	.1306	.0179
ESM 1040	2.72	46	.362	.1633	.0213
ESM 1004XII	1.71	23	.344	.2161	.0183
RTV 630	3.7	80	.36	.1285	.0326
ESM 1004AP	2.19	35	.429	.1458	.0183
RTV 560	5.72	88	.429	.1515	.0465
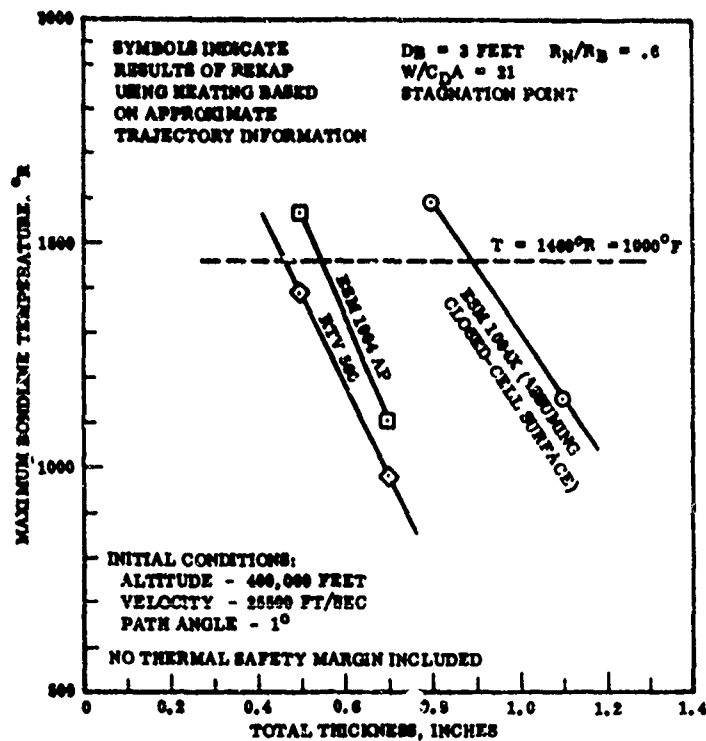
Figure 8. REKAP Predictions of Thermal Response for Three Well Characterized Ablators
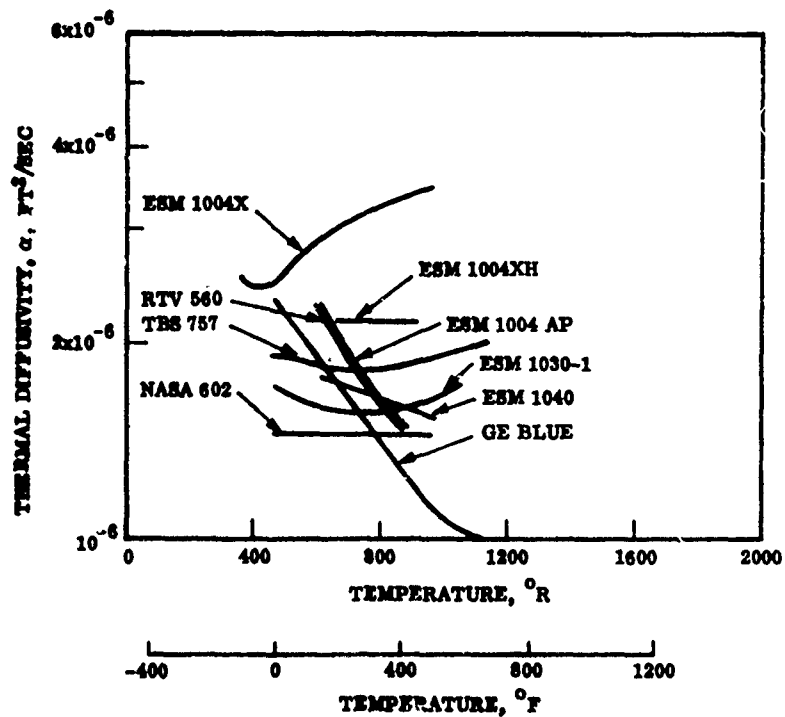
Figure 9. Thermal Diffusivity of Various Materials
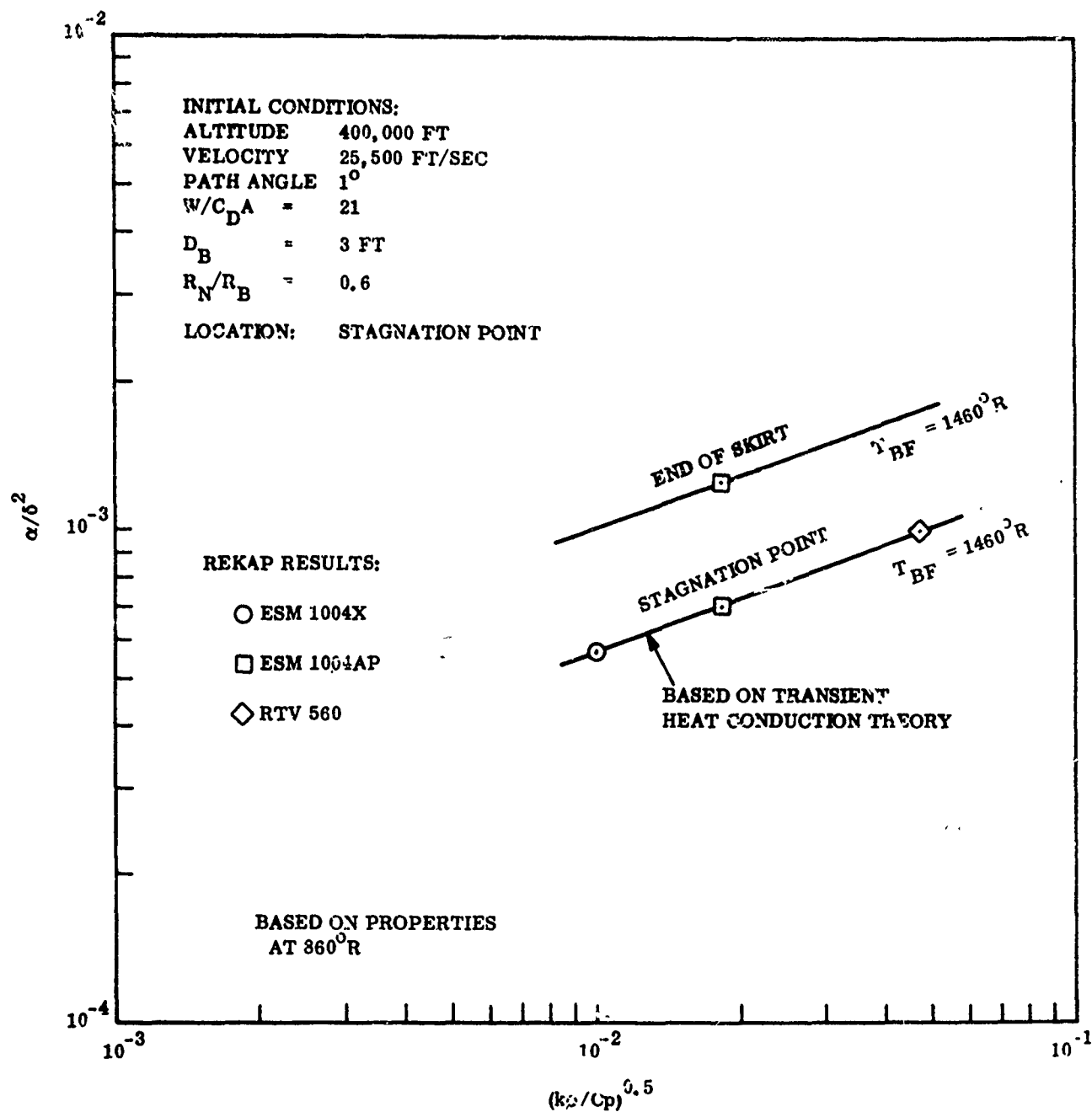
Figure 10. Insulative Thickness as a Function of Material Properties

The figure shows a log-log plot with α/δ^2 on the vertical axis (ranging from 10^{-4} to 10^{-2}) and $(k\rho/Cp)^{0.5}$ on the horizontal axis (ranging from 10^{-3} to 10^{-1}).

INITIAL CONDITIONS:
ALTITUDE   400,000 FT
VELOCITY   25,500 FT/SEC
PATH ANGLE 1°
$W/C_D A$ = 21
D_B = 3 FT
R_N/R_B = 0.6

LOCATION: STAGNATION POINT

END OF SKIRT — $T_{BF} = 1460^{\circ}R$

STAGNATION POINT — $T_{BF} = 1460^{\circ}R$

REKAP RESULTS:
○ ESM 1004X
□ ESM 1004AP
◇ RTV 560

BASED ON TRANSIENT
HEAT CONDUCTION THEORY

BASED ON PROPERTIES
AT $860^{\circ}R$

is presented in Figure 12. A REKAP prediction was made using a thickness of RTV 560 representative of the degradation depth, over ESM 1004X. Note that 40 percent of the total thickness is RTV 560. Note also, that rather than minimizing the thickness, the resultant is 40 percent of the way between the thickness requirement for RTV 560 and that for ESM 1004X. It is concluded, therefore, that the minimum thickness composite would be one consisting solely of RTV. Similarly, it can be concluded that the lowest weight composite is one consisting of ESM 1004X with only sufficient overlay to prevent a problem from high surface porosity or where surface recession is controlled, as discussed below.

2.9 EFFECT OF SURFACE RECESSION ON PERFORMANCE

For the class of silicone ablators under consideration, surface recession increases with the peak heat flux and the time-width of the heat pulse. Since time-width is strongly affected by path angle and is relatively insensitive to ballistic coefficient, as can be seen in Figure 2, surface recession, if it exists, will be greatest for an entry with a path angle greater than 1°. Since the time-width of the heat pulse decreases, Figure 2 cannot be used to select the entry conditions which will result in the greatest surface recession. As will be shown, selection of that point is not necessary to evaluate relative thickness requirements of the shield materials, as surface recession is predicted to be insignificant on the foldable portion of the shield throughout the entry corridor.

Figure 13 shows the surface temperature at which surface recession has been observed to commence for various densities of ESM and shows surface temperature as a function of heat flux. It is noted in Figure 14 (which is the result of REKAP predictions for an RTV 560 over ESM 1004X composite for a trajectory with $W/C_DA = 21$, $\gamma_E = 1^{\circ}$) that predicted peak wall temperature during re-entry is significantly reduced by even a thin layer of the higher density material. Thus, by using a sufficient layer of high density material on the surface, a significantly higher heat flux is required to initiate surface recession. Referring to Figures 3 and 13, it can be seen that on the folding portion of the shield, aft of the sphere-cone tangency point, surface recession is not expected for path angles of less than 5.6°, if a high density silicone elastomer is used on the shield surface.

It is noted that this analysis regarding surface recession is based upon the approximate heating parameters of the CREWS program. Phase II analysis using more precise techniques may indicate that some surface recession can occur at the highest path angles; however, since the time-width of the heat pulse is narrow at high path angles, total surface recession, if it exists, will be slight. The effect of vehicle size on surface recession is seen in Figure 15, which shows approximate values of heating at the sphere-cone tangency point as a function of vehicle size (assuming a constant W/C_DA). Note that the peak heat fluxes on the foldable portion of the shield decrease as shield size increases. Thus, no surface recession will occur on the skirt of the larger vehicles. Note also that the 3 foot base diameter vehicle has the largest thickness requirements (insulative thickness decreases with decreasing time-integrated heating).
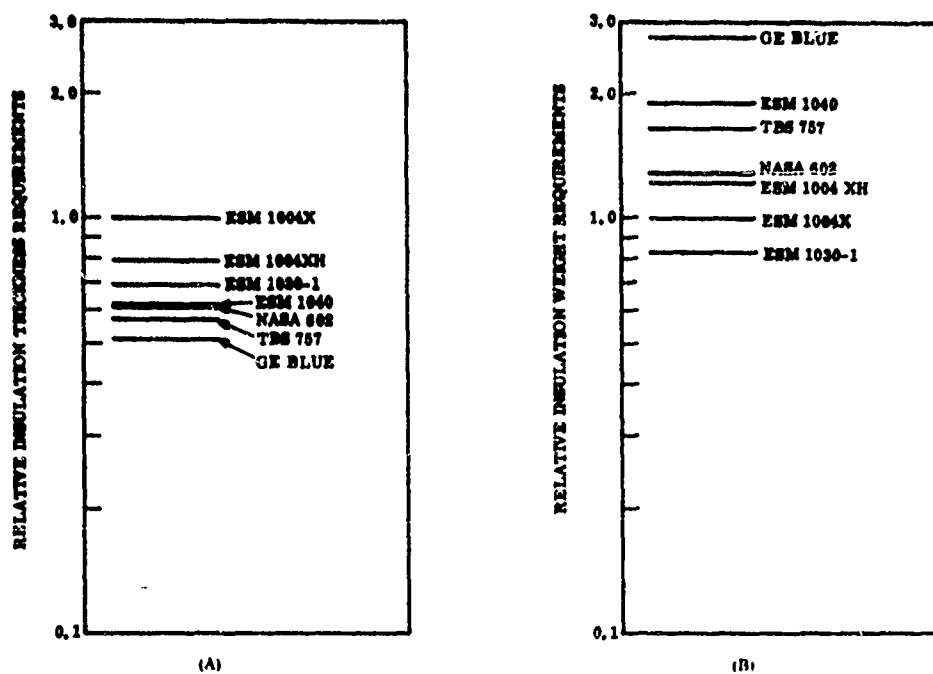
Figure 11. Predicted Relative Thermal Requirements for Various Materials
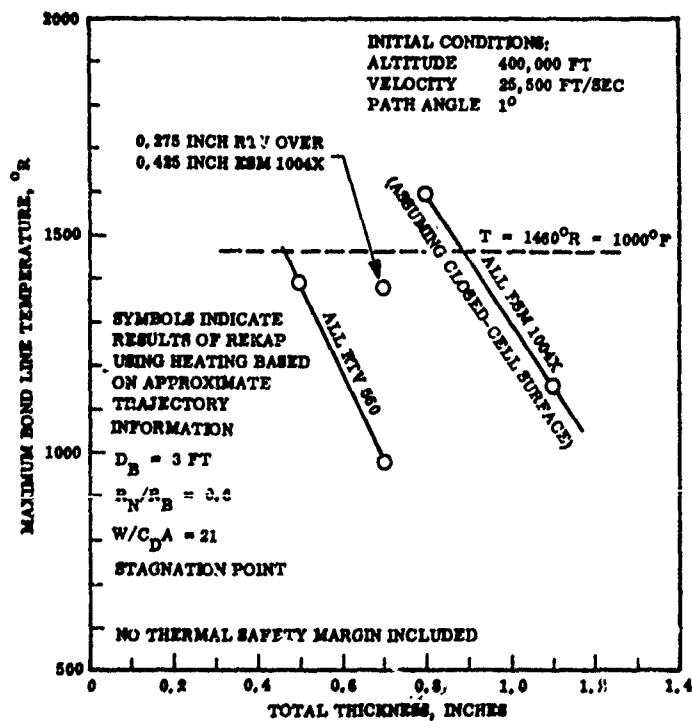
Figure 12. Effect of Variation of the Proportion of High Density Overlay
Material in a Composite Shield System

17
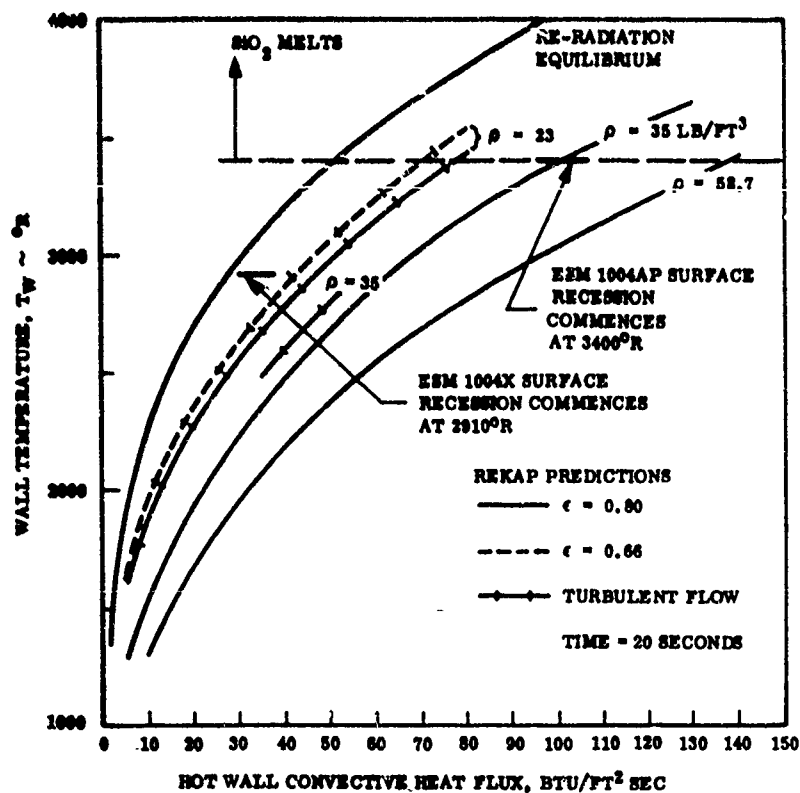
Figure 13. Variation of Surface Temperature with Convective Heat Flux
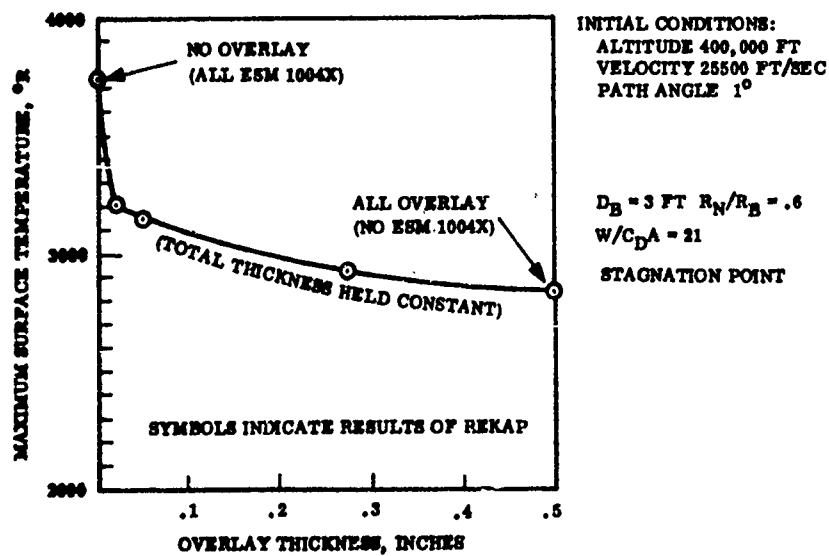
Figure 14. Effect of Overlay Thickness on Surface Temperature

18
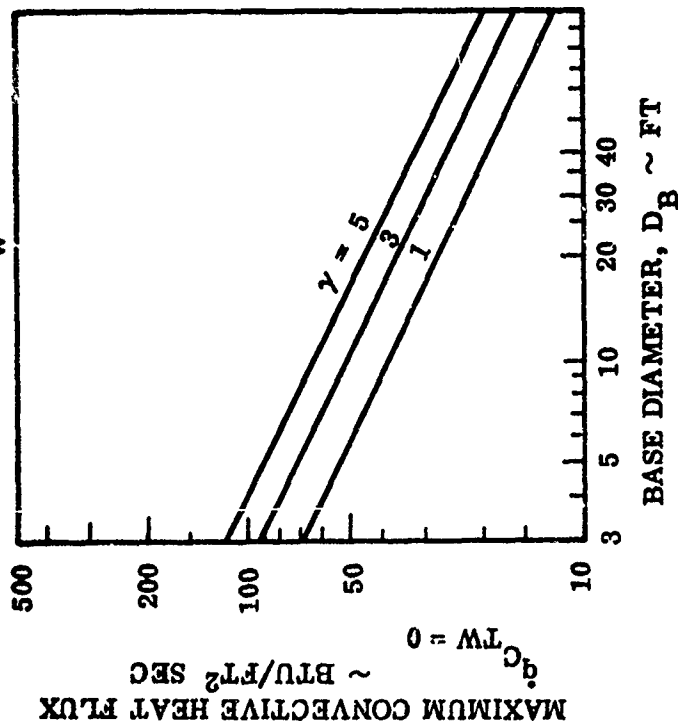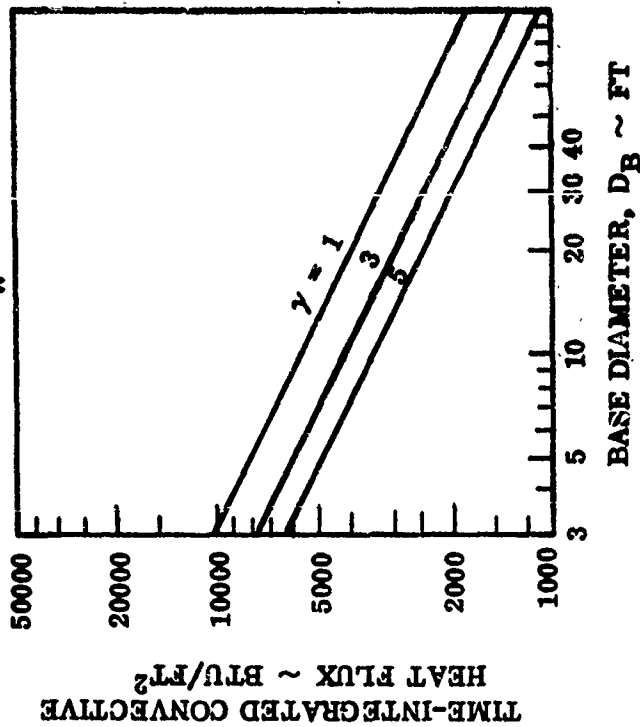
Figure 15. Approximate Effect of Vehicle Size on Heating

The relative thicknesses shown in Figure 11 are therefore considered to be valid for use in selecting the shield material throughout the entry corridor. The effect of surface recession on the thickness requirements at the stagnation point of the vehicle, as well as the possible presence of surface recession on the skirt with an increase in path angle, will be examined further as part of the Phase II effort.

2.10 SHIELD THICKNESS REQUIREMENTS

Based on REKAP predictions (for ESM 1004AP and ESM 1004X with high density overlay) and the relative thicknesses shown in Figure 11, preliminary estimates of shield thicknesses along the body are shown in Figure 16 for the various candidate shield systems.
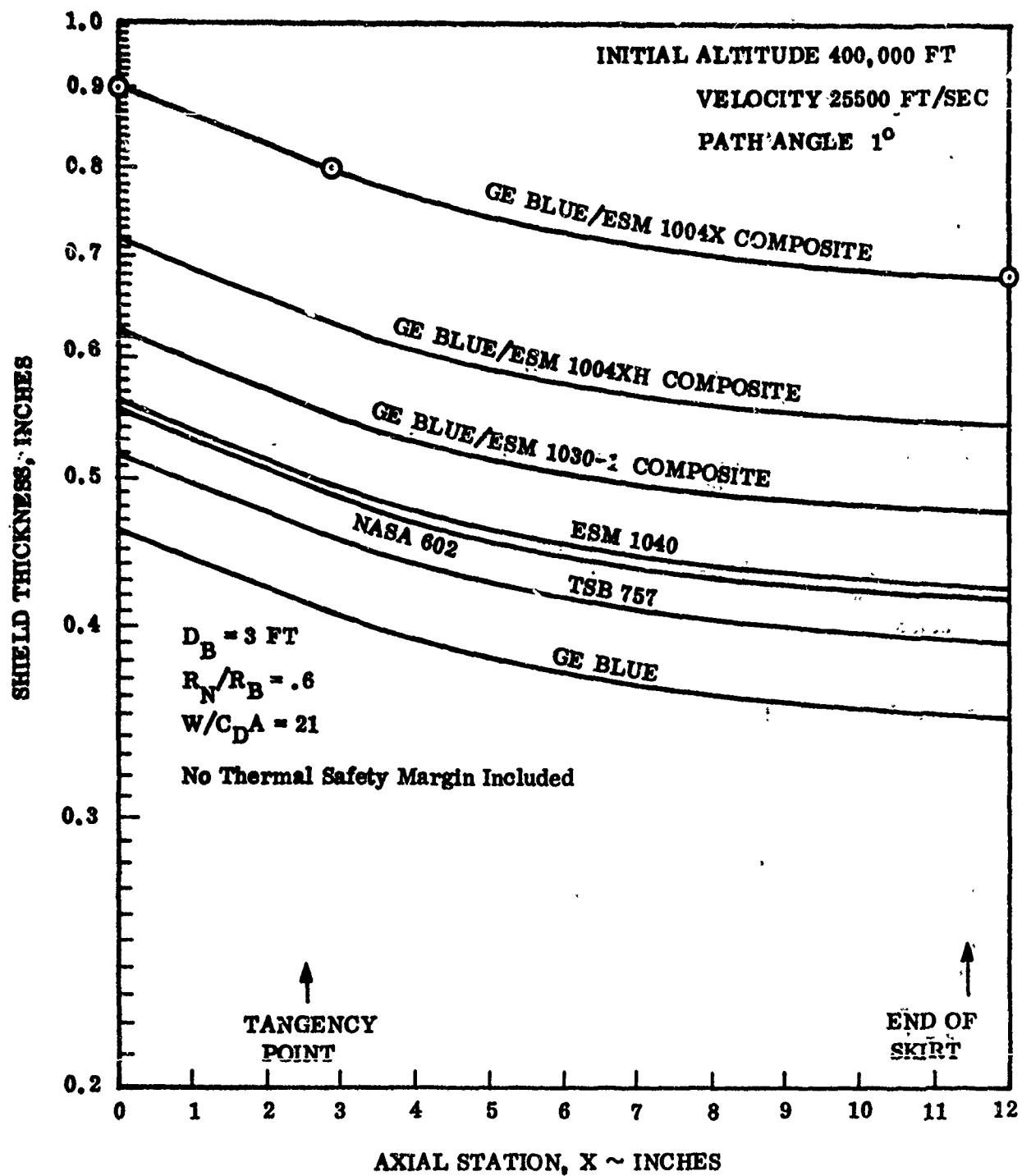
Figure 16. Estimated Shield Thickness Requirements

3. STRUCTURAL MECHANICS

Results of the contract effort to define heat shield folding techniques applicable to the ENCAP structures are presented in this section. Only preliminary drawings of the 3 foot diameter Lockheed mechanical truss vehicle were available and utilized. No details of the Goodyear AIRMAT vehicle were available so it can only be assumed that the techniques considered and commentary on each are jointly applicable to both structures.

3.1 FOLDING REQUIREMENT

The Lockheed folding structure consists of twelve folding ribs pinned at the forward section to an inner base ring and having folding capability of approximately 50 degrees. The aft section of the ribs is attached to a folding base ring. Internally mounted in the structure is a 6 inch diameter parachute canister. In the deployed position the structure with heat shield and supporting membrane attached approximates a 50 degree half angle sphere cone structure having a 3 foot base diameter. The heat shield and supporting membrane are in a tension field in the deployed position by means of a preset diameter wire cable pulling the composite over the aft end.

The stowage container for this structure is a cylinder having an inside diameter of 15.875 inches. When stowed within this diameter, the structure can be theoretically folded to between approximately a 10 degree half angle sphere cone having a base diameter of 12 inches and a 14 degree half angle sphere cone having a base diameter of 15.3 inches. To fold to the 10 degree half angle cone configuration requires that the base ring be rotated out of plane as it is folded. It is not known whether this can in fact be accomplished or, if so, with what degree of difficulty. Base ring linkage interference appears to be the limiting item with respect to folded diameter.

If the structure can be folded to the 12 inch base diameter configuration there would be available approximately a 2 inch annulus for packaging of the heat shield external to the structure. If, however, linkage binding and/or interference occurs and the structure can only be folded to the 15.3 inch diameter configuration the only packaging volume available in the vicinity of the aft ring would be internally, between the linkage. Figures 17 through 20 show the structure in the deployed configuration and in the stowed configuration, considering both extremes, and indicate available packaging area.

Figure 17. Lockheed Folding Structure

COMPOSITE HEAT SHIELD
DEVELOPED LENGTH = 9.46"
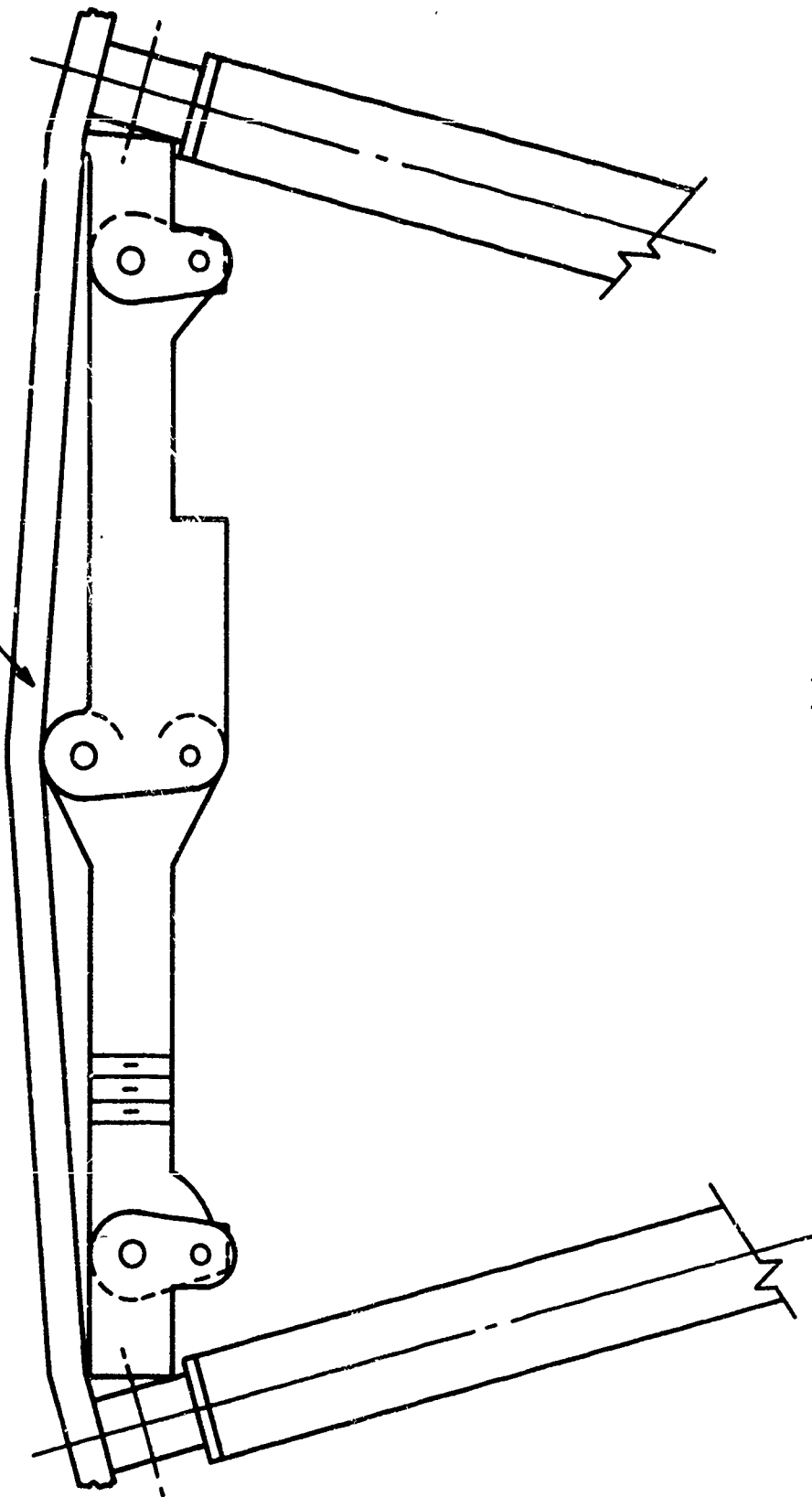
SECTION "A-A"
DEPLOYED POSITION

Figure 15.   Structure in Deployed Position (50°)

24

AVAILABLE
FOR
PACKAGING

SECTION "B-B"
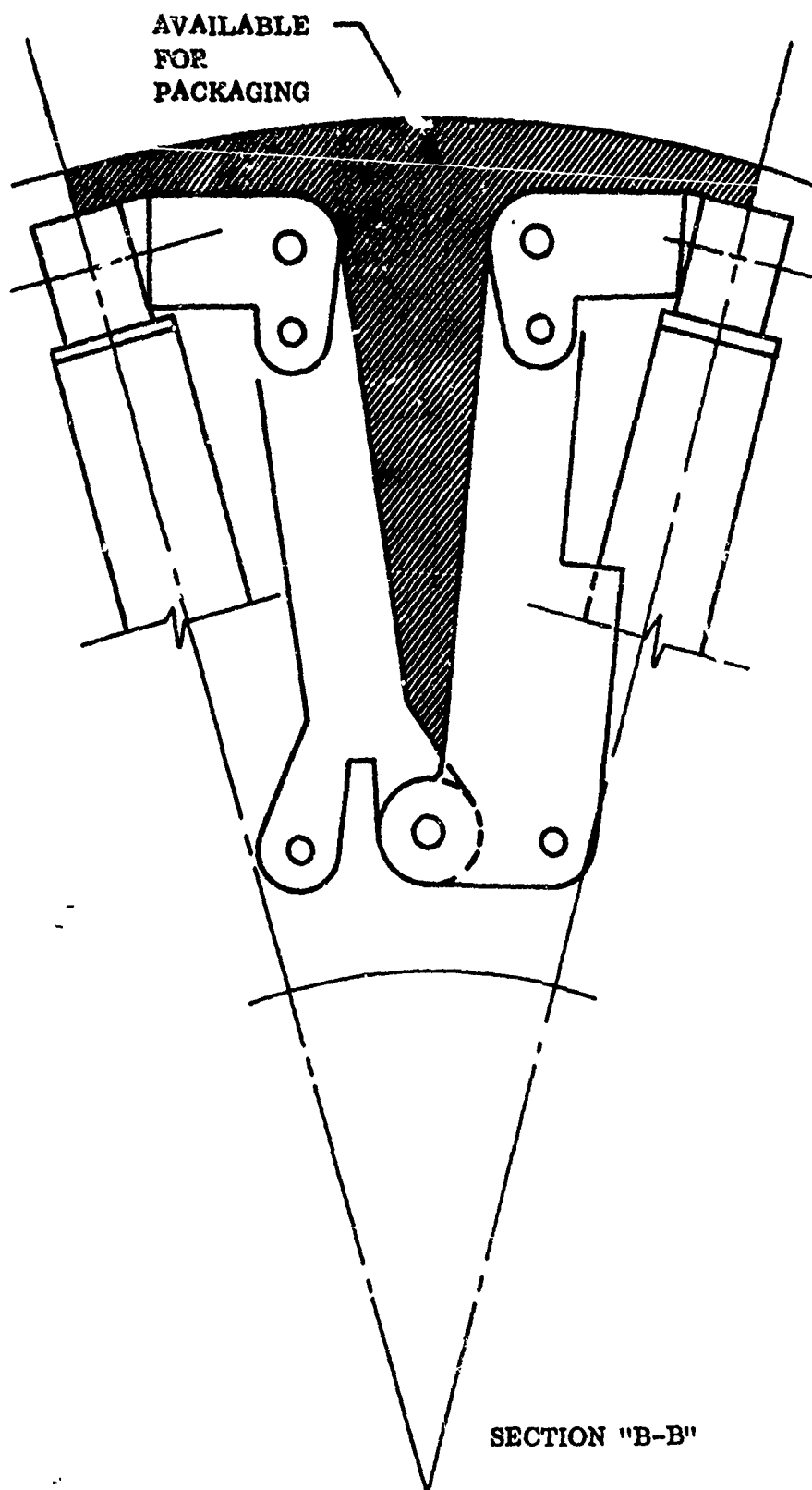
Figure 19. Structure in Stowed Position (15°)

AVAILABLE
FOR
PACKAGING

SECTION "C-C"
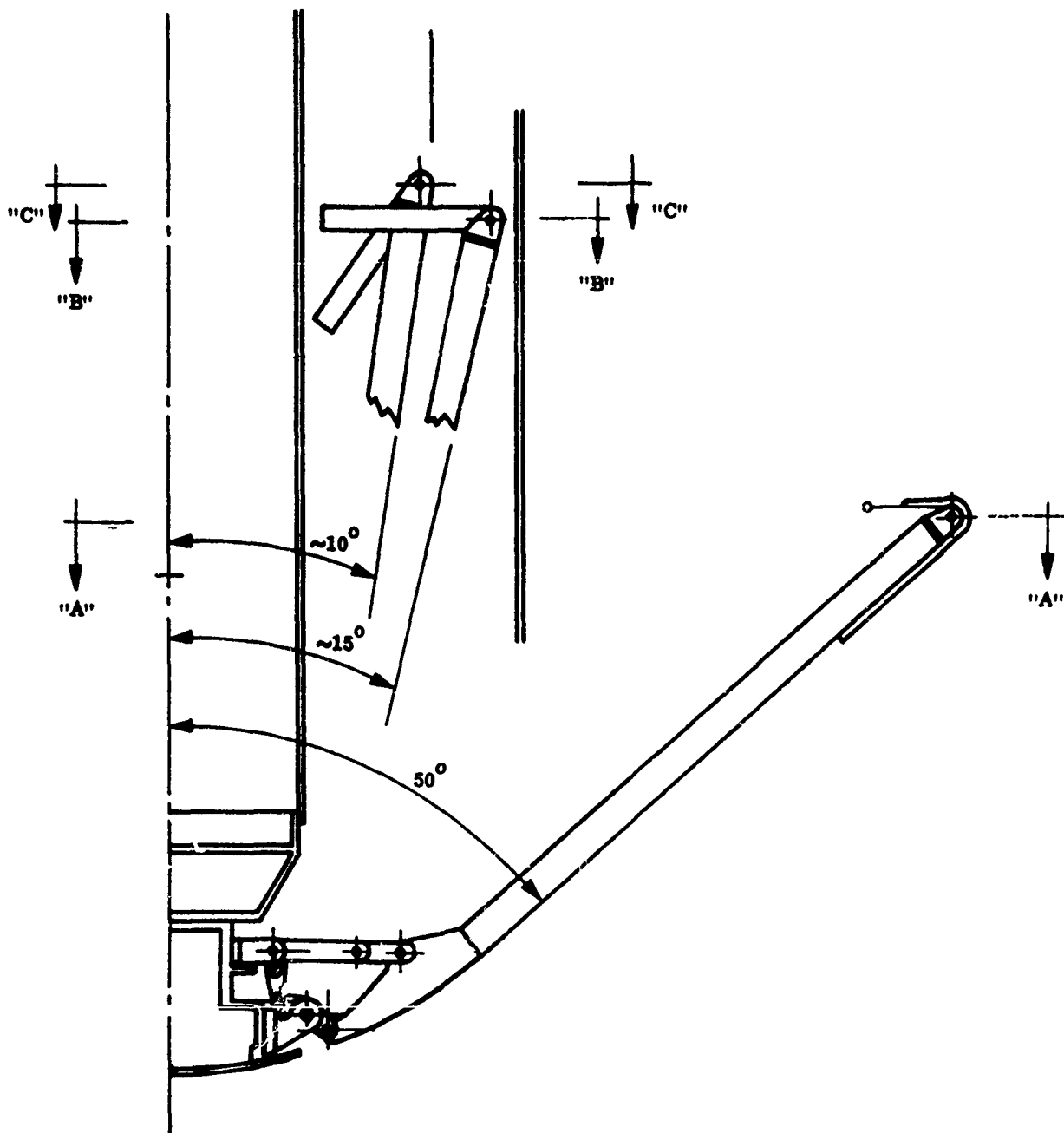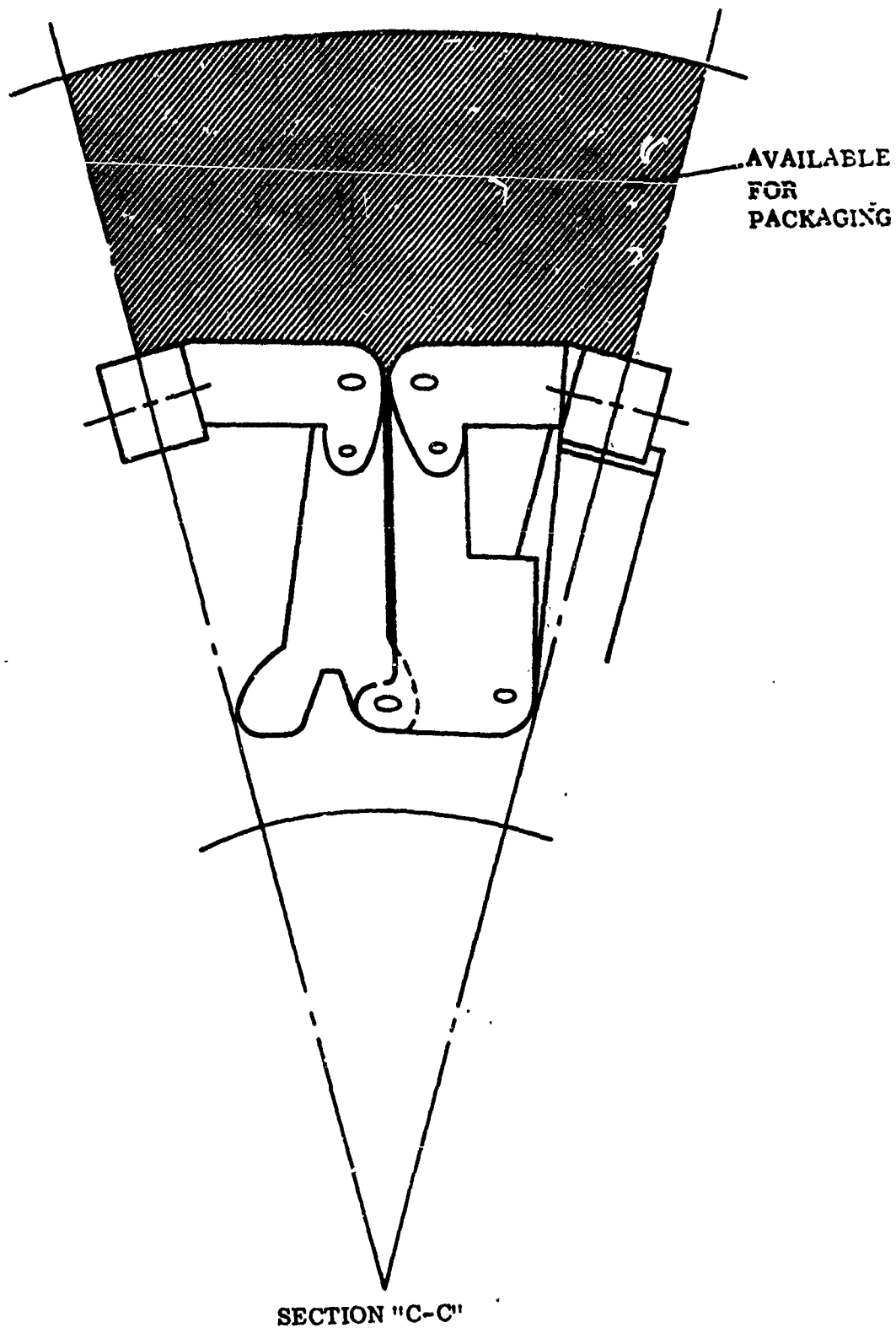
Figure 20. Structure in Stowed Position (10°)

26

3.2 HEAT SHIELD FOLDING CONCEPTS

To establish a preferred method of folding a heat shield material within the packaging volume available in the stowed condition, five folding concepts have been considered. The advantages and disadvantages of each are discussed below.

Of all the arrangements considered there are only two which show sufficient merit for consideration, namely, composite bending and the slit shield. It is recommended that the composite bending arrangement be selected as the preferred approach and that the shield be slit at selected locations if bend radius becomes critical. Additional flexibility can be achieved in the composite arrangement by consideration of such techniques as coring to remove material thereby effectively reducing the system modulus.

3.2.1 Composite Bending (Figure 21a)

In this arrangement the heat shield is completely bonded to the wire cloth membrane. A thin overlay material may be required for the heat shield to improve its tear resistance and notch sensitivity. In considering this system it has been assumed that the heat shield extensional stiffness is very small compared to the wire cloth and overlay. With this assumption it can be qualitatively stated that there will be insufficient lateral support for the outer facing loaded in compression and that local buckling of the facing will occur. This will have the tendency to shift the neutral axis of the composite toward the facing loaded in tension minimizing tensile strain and tear probability. The advantages and disadvantages of this concept are as follows:

Advantages

- Continuous heat shield
- Continuous bonding of shield to membrane
- Relatively easy fabrication

Disadvantages

- Requires flexible heat shield material
- Minimum bend radius restrictions
- Post buckled state of compression face
- Permanent set in folded condition must be overcome during deployment.

3.2.2 Slit Shield (Figure 21b)

In this arrangement the shield is similar to the composite arrangement with the addition of slits. The slits increase the flexibility of the system in positive bending. In negative bending the behavior is identical to composite bending. The degree of flexibility increase is a function of the number and spacing of the slots. If slots are spaced sufficiently close, the interaction of the heat shield material and cloth could be minimized and a rigid heat shield material utilized. The advantages and disadvantages of this concept are as follows:

27

A-COMPOSITE BENDING
OVERLAY (OPTIONAL)
HEAT SHIELD
WIRE CLOTH
N.A.
POSITIVE
N.A.
NEGATIVE

B-SLIT SHIELD
OVERLAY
HEAT SHIELD
WIRE CLOTH
N.A.
POSITIVE
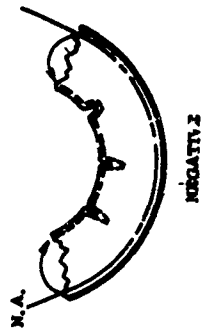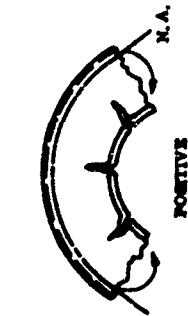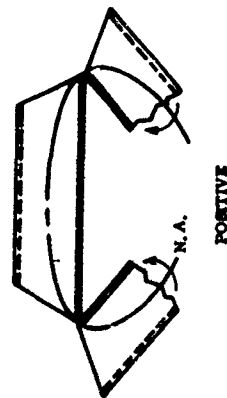
Figure 21a. Heat Shield Folding Concepts

C-SLIT SHIELD LINE ATTACHED
OVERLAY
HEAT SHIELD
WIRE CLOTH
LOCAL BOND
NEGATIVE
POSITIVE

D-ACCORDIAN
HEAT SHIELD
WIRE CLOTH
LOCAL BOND

E-LAMINATED
HEAT SHIELD LAMINATES
WIRE CLOTH
ATTACHMENT ℄
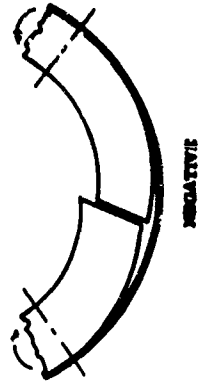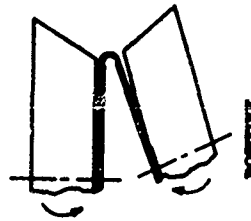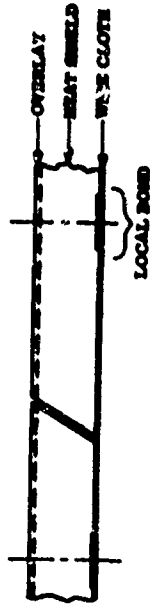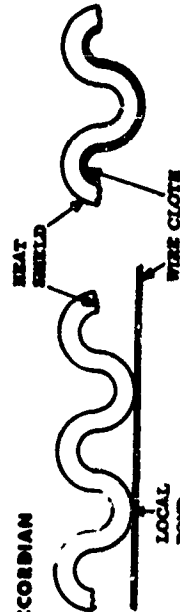
Figure 21b. Heat Shield Folding Concepts

28

Advantages

- In positive bending minimum bend restriction can be eliminated locally
- Allows use of rigid heat shield materials
- Reduces tensile strains in heat shield material
- Forces to overcome permanent set in folded condition are reduced.

Disadvantages

- Heat shield surface is discontinuous
- High bond peel stresses at discontinuity
- Increased manufacturing complexity.

3.2.3 Slit Shield Line Attached (Figure 21c)

This arrangement is similar to the slit shield except the heat shield sections are attached only over a narrow band. Although it appears that flexibility may be increased there is no reliability in such a system and it should not be given further consideration.

3.2.4 Accordion (Figure 21d)

Both concepts depicted have increased bending flexibility but have the major disadvantage of having an irregular surface during flight. Packaging volume to accommodate the corrugations would also be prohibitive. This arrangement should be given no further consideration.

3.2.5 Laminated (Figure 21e)

In this arrangement, the heat shield is built up from thin laminates, such that shear rigidity is significantly reduced. Overall bending flexibility is increased by the factor N^2 for a constant total shield thickness, where N is the number of laminates. Each section of each laminate would be attached locally by bonding or other mechanical means, which would greatly reduce the reliability of the system. In addition, manufacturing considerations make the concept unattractive. This arrangement should be given no further consideration.

3.3 APPLICABILITY OF RECOMMENDED CONCEPTS

The two most promising concepts, composite bending and slitting of the heat shield material, have been examined to determine if they can be utilized to package the heat shield in the available volume and to determine the material bend requirements.

Figure 22 shows the condition of a heat shield in composite bending when packaged within maximum available volume. The difference between (A) and (B) is the direction of the force applied to the shield during packaging. (A) requires tangential force whereas (B) can be packaged with radial force only. Both schemes appear to be equally feasible. (A), however, does not require as small a bend radius and appears to have more capability to accommodate itself to available volume. Of these two configurations (A) would appear to be the preferred approach.

PACKAGED
BOUNDARY

(A)

PACKAGED
BOUNDARY

(B)
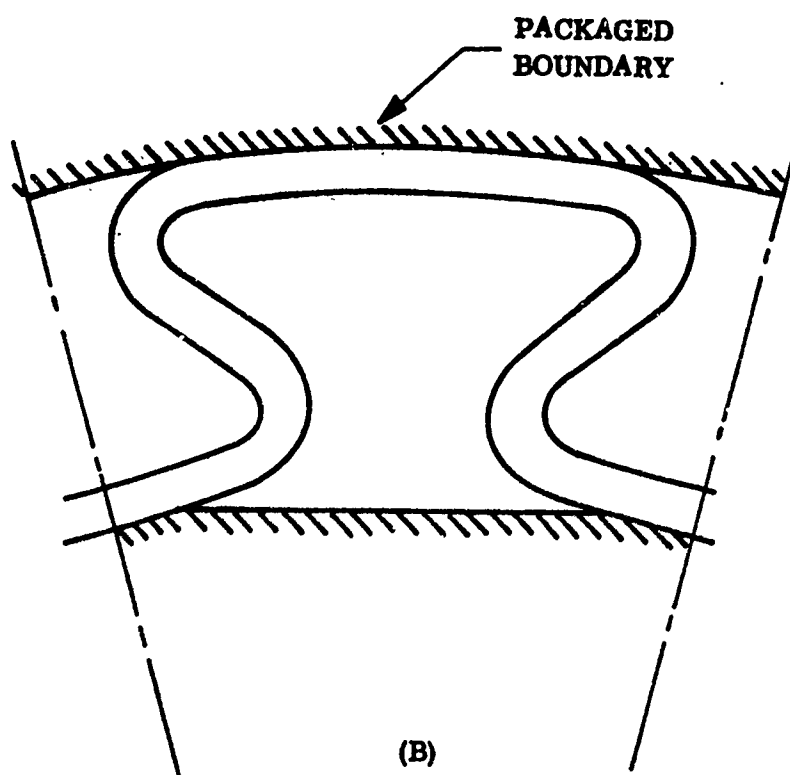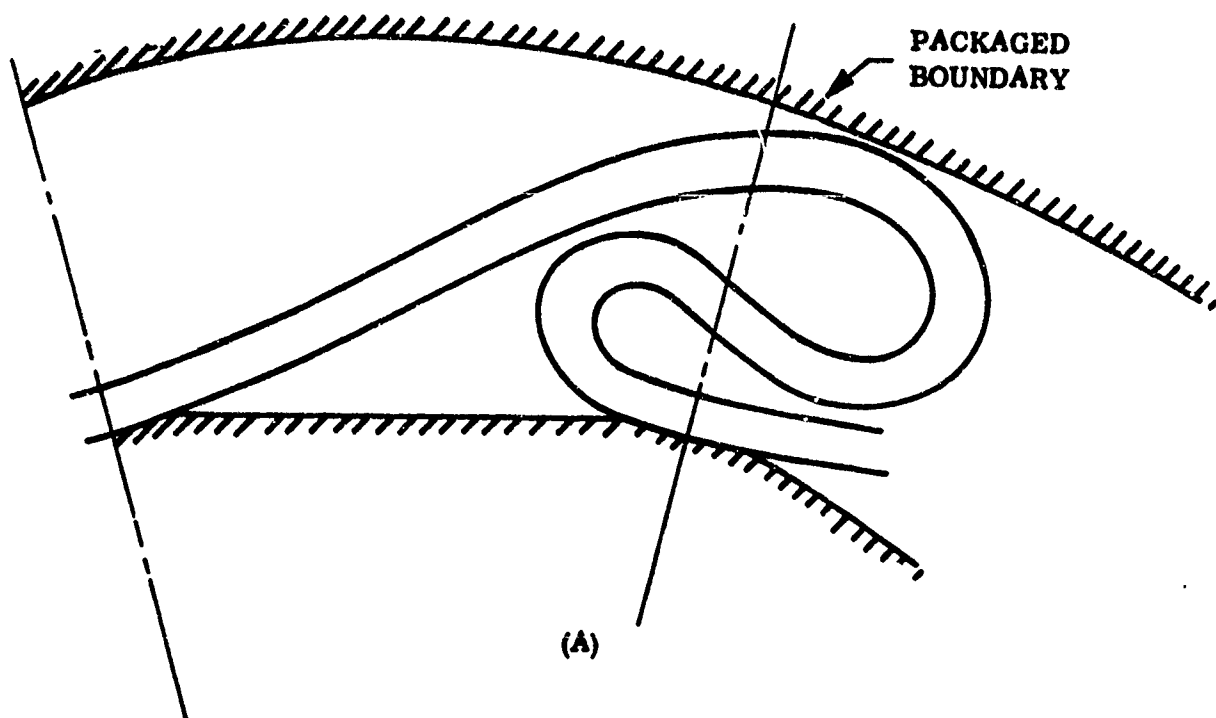
Figure 22. Heat Shield in Composite Bending

Figure 23 is the same approach as used in Figure 22 with the exception that in the areas where the heat shield is bent to small radii and the outside surface is in tension the heat shield has been slit. In (A) no advantages are obtained by slitting since the remaining bend radius remains the same. In (B), however, the addition of the slits is sufficient to relax the system and more than double the radius of the remaining bend. This arrangement therefore has appeal if the material stiffness is too great or if packaging requirements tighten. Figure 22 (A), however, remains the preferred approach.

This work was performed assuming a heat shield thickness requirement at the aft end of 1/4 inch. On this basis the composite heat shield requires a minimum bend radius capability of approximately 1/4 inch.

Two approaches have been considered in the event that the packaging annulus is prohibitively small and internal packaging must be accomplished locally at the aft end. These are shown in Figures 24 and 25. In both cases packaged volume of the heat shield is reduced. This is accomplished in Figure 24 by either thinning the heat shield locally or pinching (compressing) the material between the folded links. In Figure 25 this is accomplished by utilizing a band of heat shield material that is shorter in the packaged condition than in the deployed condition. By having intermittent adhesion to the membrane, stretching of the heat shield can taken place during deployment. The major drawback with this arrangement is that if the heat shield material should tear in the deployed condition there would be no adhesion and thermal protection at the aft end would be compromised. Both cases also require that the composite heat shield be capable of being folded back upon itself with zero radius bends. Although neither approach is very satisfactory it is recommended that the concept of Figure 24 be carried as an alternate and given additional study.

Two aspects of the packaging problem require further definition. First, is the length along the shell meridian for which the heat shield would have to be slotted. Second, is the double bend requirement of the heat shield and wire cable that wraps over the aft section. Both of these must be developed during future studies before final design selection.

3.4 FOLDABILITY RATING

It is necessary to rate heat shield materials according to their "foldability". The factors involved in establishing such a rating are:

σ_u	–	ultimate tensile strength
σ_t	–	tear strength
ϵ	–	ultimate strain
ν	–	Poisson's ratio
E	–	modulus of elasticity
s	–	permanent set
r	–	minimum bend radius
t	–	heat shield thickness

PACKAGED
BOUNDARY

(A)

(B)
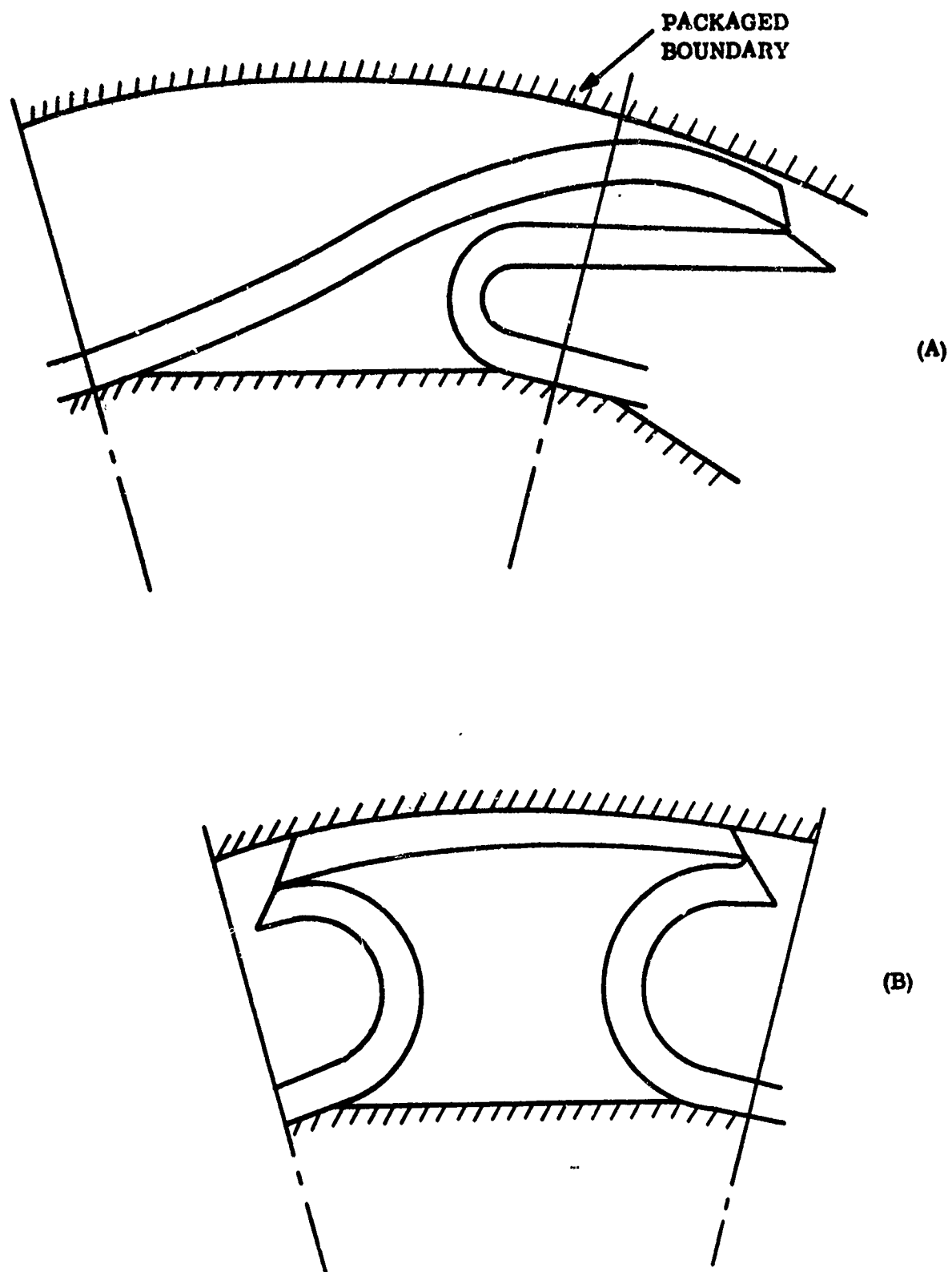
Figure 23. Heat Shield in Composite Bending and Slit

32
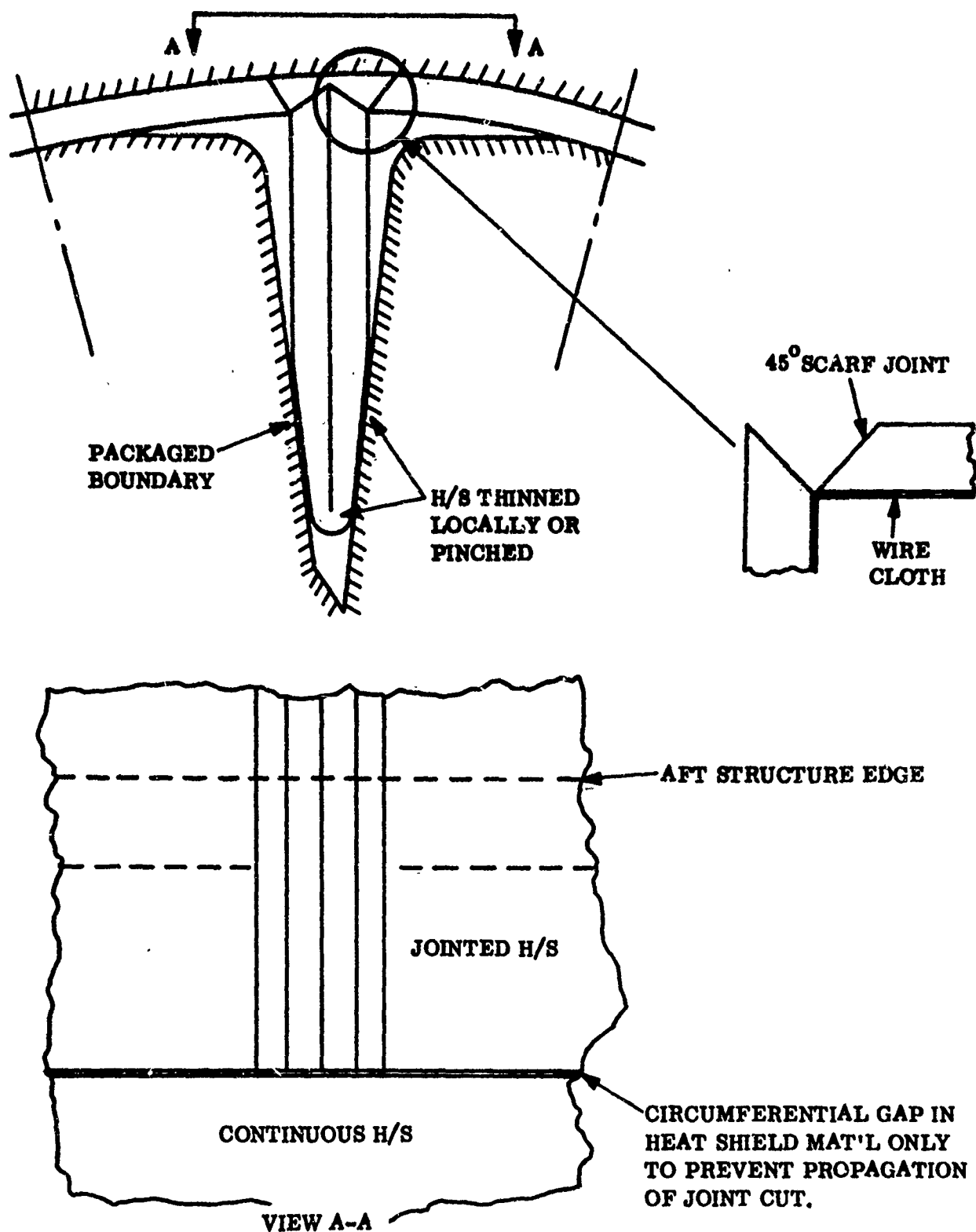
Figure 24. Alternate Approach for Aft End Packaging of Heat Shield by Thinning or Compression

WIRE CLOTH BONDED TO H/S
IN THIS AREA ONLY

H/S FABRICATED LENGTH = 8.16"
(STRETCHED LENGTH ≈ 9.46")

PACKAGED
BOUNDARY

LOCAL INSIDE OVERLAY
TO PREVENT TEARING

UNBONDED
REGION

CIRCUMFERENTIAL GAP
IN H/S ONLY TO PERMIT
INDEPENDENT FABRICA-
TION AND TO PREVENT
TRANSFER OF TENSILE
STRAIN.

CONTINUOUSLY BONDED H/S

VIEW A-A
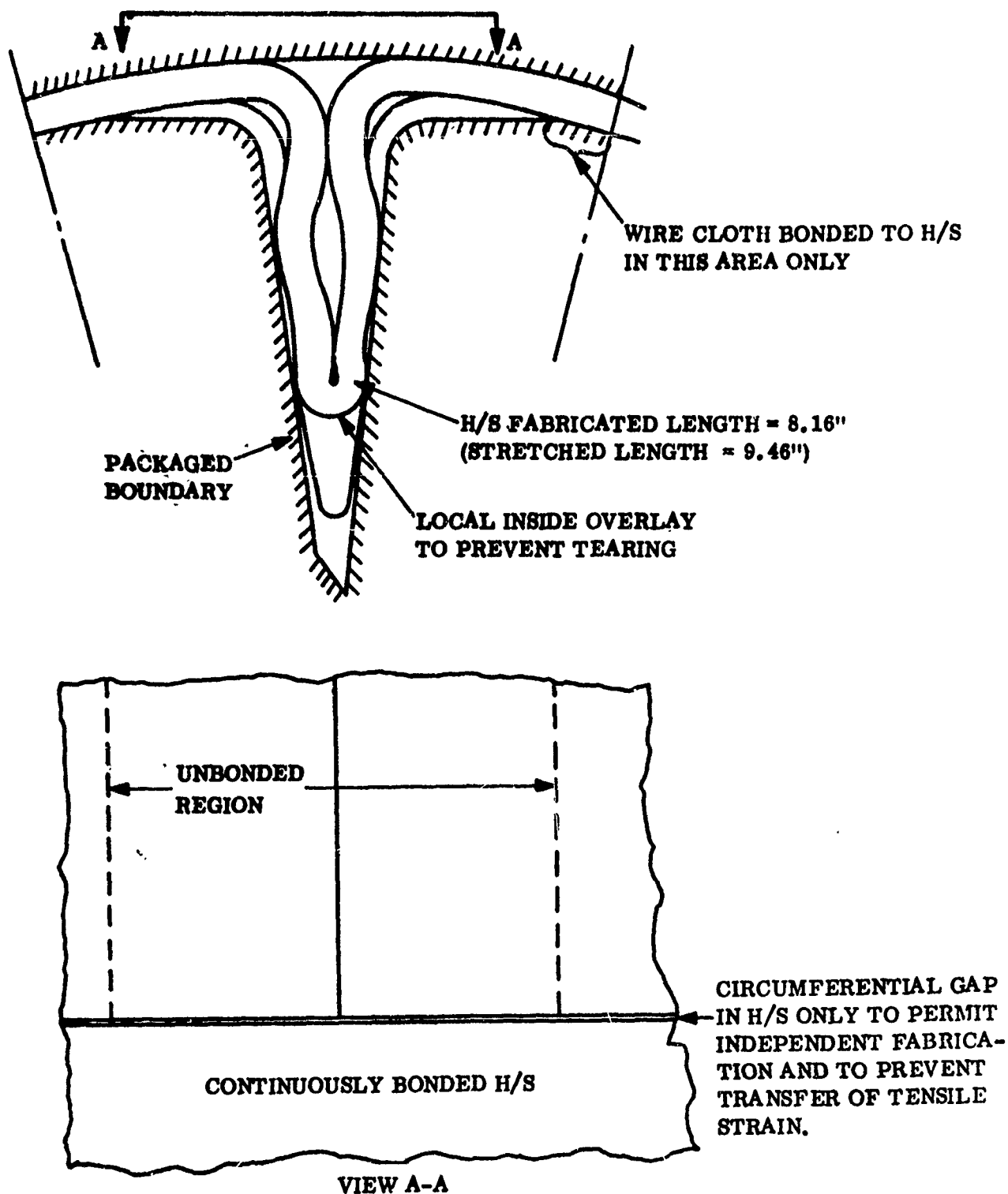
Figure 25. Alternate Approach for Aft End Packaging of Heat Shield
by Stretching

34

For a single thickness linear elastic material

$$\text{Extensional flexibility} = \frac{(1-\nu^2)}{Et} \; ; \quad \text{Recoverability} = \frac{1}{S}$$

$$\text{Flexural flexibility} = \frac{12\,(1-\nu^2)}{Et^3} \; ; \quad \text{Deployability} = \frac{1}{ES}$$

The notch resistance of a folded sheet is proportional to the tear strength and inversely proportional to the minimum bend radius:

$$\therefore \text{ assume that resistance} = k \cdot \frac{\sigma t}{r} \qquad (k = \text{constant})$$

The short term ability to deform non-linearly is proportional to the ultimate strain. The recoverability from a folded condition (deployability) is a function of the modulus change with time and temperature. Deformation tests measuring the permanent set of specimens subject to a fixed compression will give an indication of this recoverability.

Therefore, for rating purposes assume material 1, the base material, to be used as datum, is ESM 1004 X and all other single materials or composites will be related to this. For material 2 rationalizing we have:

<u>Category Ⓐ</u>

$$R_A = \text{Flexibility factor*} = \left(\frac{1-\nu_2^2}{E_2 t_2^3} \right) \left(\frac{E_1 t_1^3}{1-\nu_1^2} \right) = \frac{E_1 t_1^3}{E_2 t_2^3}$$

<u>Category Ⓑ</u>

$$R_B = \text{Notch Resistance factor} = \left(\frac{\sigma t^2}{r^2} \right) \left(\frac{r_1}{t_1} \right)$$

<u>Category Ⓒ</u>

$$R_C = \text{Deployability factor} = \frac{E_1 S_1}{E_2 S_2}$$

---

*It is likely that the Poisson's ratios for most foldable heat shield materials are similar and can be ignored in the rating.

As an example of this the A rating of ESM 1030-1 over the reference material ESM 1004 X at 100°F, assuming say 80 percent of the ESM 1004-X thickness is necessary for thermal requirements, will be

$$R_A = \left(\frac{27}{40}\right)\left(\frac{1.0}{0.8}\right)^3 = 1.32$$

(this uses the lower confidence limits on E). Therefore, the reduced thickness of 1030-1 is 32 percent more flexible than the 1004-X, despite the increase in modulus. The other ratings can be assessed when data becomes available.

For composites the flexibility factor will be modified, viz:
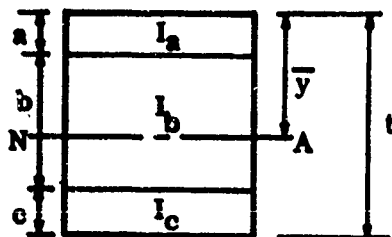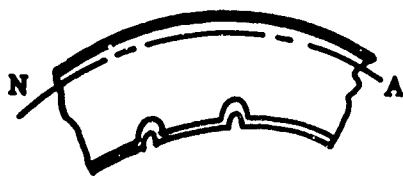
$$R_A = \frac{E_1 I_1}{E_a I_a + E_b I_b + E_c I_c}$$

where I = 2nd moment of area of each sect. For the single slap $I_1 = t_1^3/12$

For the composite slab

$$I_a = \frac{a^3}{12} + a\left(\bar{y} - \frac{a}{2}\right)^2$$

$$I_b = \frac{b^3}{12} + b\left(\bar{y} - a - \frac{b}{2}\right)^2$$

$$I_c = \frac{c^3}{12} + c\left(a+b+\frac{c}{2} - \bar{y}\right)^2$$

where $\bar{y}$ = the distance of the neutral axis from the top surface determined by setting

$$\int_{\bar{y}-t}^{\bar{y}} \frac{Eydy}{r(1-v^2)} = 0 \quad \text{or} \quad \int_A \frac{EydA}{r(1-v^2)} = 0$$

When surface buckling occurs on the inner bend surface due to the lack of lateral stiffness, then the NA will shift towards the tensile surface, material C will become ineffective and the composite will behave as a two-layer system. The net effect of this will be to reduce the outer surface tensile stresses and the subsequent tear possibility.

For composites, ratings B and C should be applied to both the outer materials if inner surface buckling is known not to occur and to the outer and center if it does.

4. MATERIALS PERFORMANCE

Base materials properties data are required to assess the relative performance characteristics of the candidate materials for application in a foldable heat shield system. Thermal properties are necessary to predict ablation/insulation performance and to size relative heat shield thicknesses. Mechanical properties are required to evaluate the foldability and structural characteristics of the proposed heat shield systems. The specific properties of interest and the temperature range of the measurements are shown in Table 4.

The specific experimental techniques which were used to generate data as part of this program are discussed in the following paragraphs.

TABLE 4. MATERIALS PROPERTIES

Property	Temperature (^{O}F)
Thermal	
Density, ρ	80
Thermogravimetric analysis, TGA	80 → 1800
Thermal conductivity, k	80 → 500
Specific heat, C_p	80 → 500
Mechanical	
Tensile strength, σ	-200 → 300
Elongation, e	-200 → 300
Elastic modulus, E	-200 → 300
Tear strength, σ_t	80
Compression set, S	80
Minimum bend radius, R	80

4.1 THERMAL PROPERTIES

Thermal conductivities were measured using a Dynatech TC-1000 thermal conductivity comparator with a 2-1/2 inch square test specimen. Measurements were made in 1 atmosphere of nitrogen at several temperatures from 100°F to 550°F. Several test points were also obtained at reduced pressure (10^{-3} mm Hg or less).

Specific heat values were obtained at 150, 350, and 500°F in 1 atmosphere of nitrogen using the Perkin-Elmer Differential Scanning Calorimeter (DSC-1). A minimum of three 15 to 30 mg. samples of each material was tested. The reported value represents the average of the individual measured values.

Thermogravimetric analyses (TGA) were performed in vacuum (10^{-3} mm Hg or less) using approximately 20 mg test samples. Sample weight was monitored with a Cahn RF Electrobalance and recorded as a function of temperature. Test runs were made at heating rates of 10°C/min. and $5.5 - 8.5^{\circ}$C/sec. for each material studied.

Results are summarized in Table 5.

TABLE 5. THERMAL PROPERTY DATA SUMMARY

Property	ESM 1004-X	ESM 1030	ESM 1004-XH	NASA 602	TBS 757	ESM 1040	GE Blue
Density, ρ (lbs/ft^3)	15	18	23	35	43	46	80
TGA 10 percent weight loss	770°F	750°F	870°F	700°F	900°F	600°F	950°F
50 percent weight loss	1170°F	980°F	1280°F	810°F	–	930°F	–
w/wo at 1600°F	0.37	0.15	0.42	0.26	0.63	0.33	0.60
Thermal Conductivity, at 150°F (10^{-5} BTU/ft-sec-$^{\circ}$F)	1.24	1.28	1.50	2.05	2.00	2.70	4.82
Specific Heat, C_p at 150°F (BTU/lb-$^{\circ}$F)	0.31	0.37	0.29	0.40	0.31	0.32	0.32

4.2 MECHANICAL PROPERTIES

Tensile tests were performed to define ultimate tensile strength, elastic modulus and ultimate elongation of the candidate materials. Dumbell type specimens 6 inches long by 2 inches wide with 1 inch wide reduced gage widths were tested with an Instron test machine. Test temperatures were attained in a convection oven utilizing liquid nitrogen for low temperatures. Strain measurements were approximated

from machine crosshead displacement curves to evaluate clastic modulus and elongation. Since a limited number of samples of ESM 1040 and TBS 757 were available, some of the tensile property functions for these materials were predicted based on the known behavior of similar materials.

Compression set characteristics were measured using the basic technique described in Federal Test Method Standard No. 601, Method No. 3311. Round specimens (1.625 inches diameter) approximately 1/2 inch thick were compressed to a thickness of 0.250 inch. Specimens were maintained in this state, at room temperature, for eight days after which the compressive force was removed. Final thicknesses were measured 20 minutes after removal of the compressive force. Where sufficient samples were available, measurements of compression set were made after two days and/or four days. In all cases compression set, S, was calculated as a percentage of the original compressive strain, i.e.,

$$ S = \left[\frac{t_o - t_f}{t_o - t_c} \right] \quad (100\ \%) $$

Where: t_o = initial thickness

t_f = final thickness

t_c = compressed thickness = 0.250 inch

Minimum bend radii were established using 2 inch by 4 inch test specimens which contained opposing 1/2 inch long slits at the center of the 4 inch edge. These slits were included to simulate a flaw in the material which would provide a tear propagation site. These specimens were bent and fastened around cylinders of various radii and the width of untorn material between the slits was measured as a function of time for up to eight days. An arbitrary failure criterion of tear propagation through one-third of the initial specimen width between slits in eight days time was used to establish minimum bend radii. The minimum bend radius for which a material can survive the failure criterion was estimated by interpolation of the measured test data and is reported as the minimum bend radius.

The tear strength of each of the candidate materials was determined by the technique of Federal Test Method Standard No. 601, Method No. 4711, using the die C specimen. These tests were performed in an Instron test machine.

Results are summarized in Table 6.

4.3 MATERIAL SELECTION TRADEOFF

Since any of the candidate heat shield material systems can be sized to provide adequate thermal protection for the entry conditions under consideration, the material selection tradeoff criteria can be limited to foldability, weight, and overall thickness. In order to perform a meaningful tradeoff analysis, it is desirable to obtain quantitative rating factors for each tradeoff criterion for each candidate system. This approach is discussed in the following paragraphs.

TABLE 6. MECHANICAL PROPERTY DATA SUMMARY

Property (Average Value at 80°F)	ESM 1004-X*	ESM 1030*	ESM 1004-XH*	NASA 602	TBS 757	ESM 1040*	GE Blue*
Density, ρ (lbs/ft³)	15	18	23	35	43	46	80
Tensile strength, σ (psi)	9	20	24	35	84	88	670
Elastic modulus, E (psi)	43	45	60	1650	290	200	1190
Elongation, e (percent)	22	45	39	4	27	47	54
Tear Strength, σ_t (lb/in.)	2.4	2.1	4.2	5.4	18.2	17.6	45
Compression set, S (percent)	5.8	2.0	9.2	30	7.9	11	3.6
Minimum bend radius, R (thickness fraction)	1.6	1.9	2.3	15	2.5	1.5	1.9

*After 8 days at 50-percent compressive strain

4.3.1 Foldability

The foldability of candidate heat shield systems may be considered to be a function of three factors:

1) Flexibility - the ease with which the material system is initially folded.

2) Tear resistance - the ability of the system to resist tearing and maintain its structural integrity in the folded state.

3) Recoverability - the ability of the system to resist permanent deformation in the folded condition which would impair its capability to return to its initial geometry upon unfolding.

40

For a single thickness of a linear elastic material, flexural flexibility can be given by:

$$F = \frac{1 - \nu^2}{EI}$$

Where:
ν = Poisson's ratio
E = elastic modulus
I = moment of inertia

Thus, we can can define a flexibility factor, R_A, by normalizing F for a given material system to some reference system,

$$R_A = \frac{F_2}{F_1} = \frac{E_1 I_1}{E_2 I_2}$$

The $(1 - \nu^2)$ term vanishes since Poisson's ratio is assumed equivalent for all materials under consideration. For a two layer composite, R_A must be modified,

$$R_A = \frac{\left[E_a I_a + E_b I_b \right]_1}{\left[E_a I_a + E_b I_b \right]_2}$$

Where:
I = 2nd moment of area of section
a, b = overlay, ablator
1 = reference system
2 = system under evaluation

The above equation was used to obtain a quantitative flexibility rating for each of the candidate heat shield systems.

Tear resistance, N, is proportional to tear strength and inversely proportional to minimum bend radius,

$$N = k \frac{\sigma_t}{r}$$

Normalizing this tear resistance rating to a reference system, we have

$$R_B = \frac{N_2}{N_1} = \left(\frac{\sigma_2}{\sigma_1} \right) \left(\frac{r_1}{r_2} \right)$$

Where:
σ_t = tear strength
r = minimum bend radius

This equation was used to compute a tear resistance factor, R_B, for each candidate heat shield system.

Recoverability, as defined earlier, is inversely proportional to compression set. Thus, a recoverability factor, R_C, can be derived yielding:

$$R_C = \frac{S_1}{S_2}$$

Where: S = compression set

4.3.2 Weight and Thickness

In a similar manner, weight (R_W) and thickness (R_T) factors can be calculated, viz:

$$R_W = \frac{W_1}{W_2}$$

$$R_T = \frac{T_1}{T2}$$

Where: W = total system weight
         T = total system thickness

4.3.3 Tradeoff Summary

The five rating factors discussed above were computed for each of the candidate material systems using the mechanical property data in Table 6. An overlay thickness of 0.020 inch was used for the three composite systems. ESM 1004X with a GE Blue overlay was chosen as the reference system since ESM 1004X is probably the best characterized material under consideration. The results of those computations are shown in Table 7. The right hand column in this table gives the average ratio factor for each material. GE Blue/ESM 1030 is observed to have the highest overall average rating as well as the highest average rating in four of the five rating categories. Thus, unless overall thickness is weighted far more heavily than any of the other criteria, GE Blue/ESM 1030 is clearly the superior system relative to the criteria considered here.

Based on this tradeoff analysis, GE Blue/ESM 1030 is the selected heat shield system. It should be pointed out, however, that further thickness definitions may possibly make it desirable to re-evaluate this selection if the total thickness gives rise to additional constraints such as might result from packaging restrictions.

4.4 FLEXIBLE SILICONE ABLATOR SERIES 1040 (FSA-1040)

Studies performed during this contract included a comparison of data with proprietary thermal protection material designated ESM-1040.

TABLE 7. MATERIAL TRADEOFF

System[1]	R_A	R_B	R_C	R_W	R_T	$\bar{R}$ [2]
GE Blue/ESM 1004-X	1.00	1.00[3]	1.00	1.00	1.00	1.00
GE Blue/ESM 1030	2.25	1.00[3]	2.90	1.18	1.43	.1.75
GE Blue/ESM 1004-XH	1.51	1.00[3]	0.63	0.84	1.25	1.05
NASA 602	0.30	0.02	0.19	0.70	1.63	0.57
TBS-757	2.05	0.30	0.73	0.66	1.71	1.09
ESM 1040	2.17	0.50	0.53	0.57	1.58	1.07
GE Blue	0.70	1.00	1.61	0.39	1.91	1.12

Notes: (1) GE Blue Overlay thickness = 0.020 inch

(2) Average of five rating factors

(3) Computed for GE Blue overlay

The marginal compression set and the low residual weight fraction data reported in Tables 5 and 6 combined with density control difficulties experienced during fabrication led to an extensive change in the chemistry of our flexible ablator system.

The new material developed has been given the designation of Flexible Silicone Ablator Series 1040 (FSA-1040).

FSA-1040 is based on the addition polymerization silicone elastomers. These resins are known for their inherent toughness and flexibility combined with the high thermal stability typical of the silicones.

Laboratory studies thus far have shown the feasibility of producing closed cell foams within the density range from 10 - 60 lbs/ft^3. These development samples have shown flexibility far superior to any known thermal ablation material.

Insufficient ablation, thermal and mechanical property data were available at the writing of this report to factor into this study. However, tests are now in progress under the Company-sponsored program to qualify this material system for future foldable re-entry body applications.

APPENDIX
NOMENCLATURE

A	Pre-exponential factor	
C_p	Specific heat	$Btu/lbm\,^oR$
C_{pg}	Specific heat of the pyrolysis gases generated	$Btu/lbm\,^oR$
ΔE	Activation energy	Btu/lb-mole
F_a	Configuration factor	
F_e	Emissivity factor	
g	$33.2\ ft/sec^2$	
h	Enthalpy	Btu/lbm
h_a	Altitude at apogee	
h_p	Altitude at perigee	
H_{gf}	Heat of decomposition	Btu/lbm
H_K	Heat of cracking	Btu/lbm
i	Orbital inclination	degrees N of E
J	778 ft lbf/Btu	
k	Thermal conductivity	$Btu/ft\ sec\,^oR$
L	Latent heat of vaporization	Btu/lbm
$\dot{m}_g$	Time rate of generation of gases	$lbm/ft^2\ sec$
$\overline{M}_{BL}$	Average molecular weight of the boundary layer	lbm
$\overline{M}_g$	Average molecular weight of the gases injected into the boundary layer	lbm
P	Pressure	lbf/ft^2
P_r	Prandtl number	
$\dot{q}$	Heat flux	$Btu/ft^2\ sec$

$\dot{q}_{BLK}$	Heat flux blocked by escaping pyrolysis gases	$Btu/ft^2 sec$
$\dot{q}_c$	Convective heat flux	$Btu/ft^2 sec$
$\dot{q}_{HGR}$	Radiative heat flux caused by hot gas radiation	$Btu/ft^2 sec$
$\dot{q}_{NET}$	Net heat flux entering the surface	$Btu/ft^2 sec$
$\dot{q}_{RR}$	Reradiated heat flux	$Btu/ft^2 sec$
$\dot{q}_{VAP}$	Heat flux absorbed by the vaporization process	$Btu/ft^2 sec$
$\dot{q}/\Delta h$	Film coefficient $= \dot{q}_c/(h_R - h_w)$	
R	Gas constant, 1.988 $Btu/lb\text{-}mole^2 R$	
R_N	Nose radius	ft
R_B	Base radius	ft
s	Wetted length	ft
$\dot{s}$	Surface recession rate	ft/sec (unless otherwise noted)
t	Time	sec
T	Temperature	^oR (unless otherwise noted)
T_w	Surface temperature	^oR
T_m	Melt threshold temperature	^oR
u	Velocity	ft/sec
x	Depth (appendix)	ft
X	Axial station (test)	ft (unless otherwise noted)
y	Radius of body measured from the axis of symmetry	ft
δ	Thickness	ft (unless otherwise noted)
δ	Thickness of the boundary layer (appendix)	ft
δ^*	Displacement thickness	ft
ϵ	Emissivity	

η	Order of reaction	
μ	Viscosity	lbm/ft sec
ρ	Density	lbm/ft^3
ρ_c	Density of the char	lbm/ft^3
α	Solar absorbtivity	
α	Thermal diffusivity = $k/\rho\, C_p$	ft^2/sec
β	Angle measured between the earth-sun line and the orbital plane	degrees
θ_c	Vehicle half cone angle	degrees
$W/C_D A$	Ballistic coefficient	lb/ft^2
γ	Path angle	degrees
V	Velocity	ft/sec
σ	Stefan-Boltzman constant = 4.76×10^{-13} Btu/$^\circ$R^{4}ft^{2}sec	
τ	Aerodynamic shear	lbf/ft^2

Superscripts

*   Measured at the reference enthalpy conditions

Subscripts

BF   At the backface

c   Char

c   Convective

e   At the edge of the boundary layer

L   Laminar

R	Recovery Condition
T	Turbulent
v	Virgin
w	Wall
o	Stagnation condition
∞	Freestream
E	Entry condition

APPENDIX A

PLANETARY AERODYNAMIC HEATING PROGRAM (PAHP)

The PAHP program (References 6, 7, and 8) calculates heat transfer rates to the stagnation point and up to 50 body points using Lees' laminar theory (Reference 9) modified (Reference 10) to include the effect of finite pressure gardient using Blåusius' incompressible flat plate skin friction coefficients modified for compressible flow by use of Ekert's reference enthalpy parameter (Reference 11), and, in the case of the turbulent heat transfer rates, modified by Walker's turbulent theory (Reference 12) which satisfies both the momentum and energy integral equations.

$$\frac{\dot{q}_0}{h_0 - h_w} = \frac{C_0}{P_r^{2/3}} (\rho^*\mu^*)^{0.5} \left(\frac{u_\infty}{R_N} \left[\frac{\rho_\infty}{\rho_0} \left(2 - \frac{\rho_\infty}{\rho_0} \right) \right]^{0.5} \right)^{0.5}$$

$$h_0 = h_\infty + \frac{u_\infty^2}{2gJ}$$

$$\frac{\dot{q}_L}{h_{R_L} - h_w} = \frac{C_L \, \rho_e^* \mu_e^* \, y \, u_e}{P_r^{2/3} \left(\int_0^s \rho_e^* \mu_e^* u_e y^2 \, ds \right)^{0.5}}$$

$$h_{R_L} = P_r^{0.5} h_0 + \left[1 - (P_r)^{0.5} \right] h_e$$

$$\frac{\dot{q}_T}{h_{R_T} - h_w} = \frac{C_T \left(\rho_e \mu_e^* \right)^{0.2} \left(\rho_e^* \right)^{0.8} \left(\mu_e \right)^{0.5} u_e y^{0.25}}{P_r^{2/3} \left(\int_0^s \rho_e u_e \mu_e^{0.25} y^{1.25} \, ds \right)^{0.2}}$$

$$h_{R_T} = P_r^{1/3} h_0 + \left[1 - (P_r)^{1/3} \right] h_e$$

The theoretical values of the coefficients C_0, C_L and C_T are 0.707, 0.354, 0.0296, respectively, or when modified to agree with Mark 2 and RMV flight test data are 0.778, 0.389, 0.0326, respectively, (Reference 10).

On the spherical portion of the nose for which body angle is greater than 30° (body angle is defined to be 90° at the stagnation point) laminar heat transfer rates are calculated with Lee's hemispherical distribution (Reference 9).

Earth's atmospheric properties are input in table form. Rankine-Hugoniot relations are used for pressure rise across normal shock and stagnation pressure. Pressure distribution can be calculated as modified Newtonian, modified Newtonian and Prandtl-Meyer expansion, or table input of coefficient of pressure ratios as a function of body location and freestream Mach number.

Shock shape can be calculated by the method of Reference 13, which is included as a sub-routine, or can be input as a function of body locations and Mach number.

Entropy gradient effects are taken into account through a balance of the mass in the boundary layer with the mass forward of the shock and within a radius of R_s of the vehicle centerline. The equation

$$\rho_\infty u_\infty R_s^2 = 2 \rho_e u_e y (\delta - \delta^*)$$

defines the shock angle and entropy rise for the edge of the boundary layer streamline.

The equation for viscosity,

$$\mu = 24.9 \times 10^{-8} T^{0.63}$$

agrees closely with Sutherland (Reference 14) and National Bureau of Standards (Reference 15) at temperatures greater than 1000°R.

Local velocity is calculated by

$$u_e = \sqrt{2gJ (h_o - h_e)}$$

Other local properties are evaluated by isentropic expansion to the local pressure utilizing the Cornell property tables (Reference 16) in a sub-routine.

The full scale blunted Mark 2 ICBM heat sink vehicles ($0 < M_\infty < 12$), and an RMV heat sink vehicle ($6 < M_\infty < 22$), confirms the laminar and turbulent heating levels and distribution techniques using the modified heating equations.

APPENDIX B

REACTION KINETICS ABLATION PROGRAM (REKAP)

To describe the thermal behavior of a material in a re-entry environment, it is necessary to solve the transient heat conduction equation for each element of material through the char (if a char exists), the reaction zone, and the virgin material continuously and simultaneously throughout the re-entry heating period. In order to solve these second-order differential equations simultaneously, it is necessary to prescribe several boundary conditions. These boundary conditions are: (1) at the surface the net heat transfer rate to a non-permeable surface is reduced by both surface re-radiation, and the mass transfer effect of the injection of the decomposition gases into the boundary layer (blocking action), (2) at the backface of the virgin plastic or supporting substructure the heat conducted out is zero.

In general, the heat conducted into a material element is equal to the sum of the heat stored in the element, the heat absorbed in the decomposition of the material element, the heat absorbed by the decomposition gases passing through the material element, and the heat absorbed by cracking or recombination of the decomposition gases. The general heat conduction equation, valid in both the porous char and virgin material is written in cartesian co-ordinates as

$$\frac{\partial \left(\frac{K \partial T}{\partial x} \right)}{\partial x} = \rho \, C_p \frac{\partial T}{\partial t} + H_{gf} \frac{\partial \rho}{\partial t} - \left(C_{p_g} + \frac{\partial H_K}{\partial T} \right) \frac{\partial T}{\partial x} \int_{x=X}^{x=\text{BACKFACE}} \frac{\partial \rho}{\partial t} \, dx$$

$$\frac{\partial \rho}{\partial t} = \rho_v \left(\frac{\rho - \rho_c}{\rho_v} \right)^{\eta} \sum_{i=1}^{\eta} A_i \, e^{-\Delta E_i / RT}$$

At the material surface – boundary layer interface, boundary condition (1) is the thermal energy balance written as:

$$\dot{q}_{NET} = \dot{q}_c + \dot{q}_{HGR} - \dot{q}_{RR} - \dot{q}_{BLOCK} - \dot{q}_{VAPORIZATION}$$

where

$\dot{q}_c$ = hot wall convective heat flux = $\left(\frac{\dot{q}}{\Delta h} \right) \left(h_R - h_w \right)$

$\dot{q}_{RR}$ = re-radiated heat flux = $\sigma \, Fe \, Fa \, T_w^4$

$\dot{q}_{VAPORIZATION}$ = phase change energy associated with surface recession = $\rho \, L \dot{s}$

$\dot{q}_{BLOCK}$ = transpiration cooling due to injected gases

50

For laminar flow

$$\dot{q}_{BLOCK} = \dot{q}_c \left(\frac{\overline{M}_{BL}}{\overline{M}_g}\right)^{1/3} .69 \, P_r^{-1/3} \varphi_o$$

For turbulent flow

$$\dot{q}_{BLOCK} = \dot{q}_c \left(1 - e^{-0.38 \frac{C_{pg}}{C_{pBL}} \varphi_o}\right)$$

$$\varphi_o = \int_{FRONTFACE}^{BACKFACE} \frac{\partial \rho}{\partial t} \, dx \, \frac{h_r - h_w}{\dot{q}_c}$$

Surface recession can be calculated by several methods. The method chosen for a particular material depends upon ground test correlations of the material mass loss characteristics. Four such methods are:

Option 3: Surface recession is assumed to be a reaction-controlled process that can best be described by an expression of the form suggested by Munson and Spindler, Reference 17.

$$\dot{S} = \beta_1 T_w^{\beta_2} e^{-\beta_3'/T_w}$$

Option 2:

$$\dot{S} = \frac{\dot{q}_c}{\rho_w (K_1 + K_2 (h_r - h_w))} \quad \text{where } K_1 \text{ and } K_2 \text{ are constants.}$$

Option K-M:

$$\dot{S} = a \, \dot{q}_c^b (h_R - h_w)^c P_e^d \quad \text{where } a, b, c, \text{ and } d \text{ are constants}$$

Option 5: Surface recession is assumed to be occurring at a constant melt or vaporization temperature. At the surface, S is solved in the equation

$$-K \frac{\partial T}{\partial x} = \dot{q}_c + \dot{q}_{HGR} - \dot{q}_{BLOCK} - \rho_c L \dot{s}$$

so that T_w does not exceed a specified melt or vaporization temperature. Where T_w < the specified melt temperature, $\dot{s} = 0$.

At the backface of the virgin plastic or supporting substructure, the second boundary condition on the first equation is

$$K \left(\frac{\partial T}{\partial x} \right)_{BACKFACE} = 0$$

By solving the above equations simultaneously and continuously through the heating period, the surface and subsurface temperatures and material degradation time histories are obtained. The Reaction Kinetics Ablation Program (REKAP) is the mechanized numerical solution to the above model. The validity of the above approach for the prediction of the thermal response of a material undergoing thermal degradation has been proven by comparing calculated results with those obtained during ground and flight tests. A more complete description of the REKAP program can be found in Reference 18.

REFERENCES

1. Florence, D.E., "Definition of ENCAP Storage and Deployment Environments," GE/RESD PIR ARSTA 062, 16 May 1969.

2. Faust, J.W., "A Computer Program for Calculating Re-entry in Three Dimensions Assuming Instantaneous Trim," GE/RESD Fluid Dynamics Technology Component Fundamentals Memo No. 58, 6 September 1963.

3. Kohr, J., "Closed-cell ESM 1004 Surface Recession Correlations," GE ESD PIR 9151-ARSTA-051, 28 February 1969.

4. Florence, D., "Thermodynamic Ground and Flight Test Performance of a Low Density Elastomeric Silicone Formulation." GE/RESD Thermodynamics Technology Component Data Memo 110, 23 October 1967.

5. Schneider, P.J., Thermatest Laboratores, Inc., "Temperature Response Charts," John Wiley and Sons, Inc., 1963.

6. Dewees, L., "Re-Entry Vehicle Design (Ablating) Program," GE TIS R59SD391, July, 1959.

7. DiCristina, V., "Addendum to the Ablation Design Digital Computer Program," GE TIS R59SD391, March 9, 1960.

8. Dunn., J.E., "Deck Eight of Ablation Design Program," GE TFM 8151-001 LD, May 2, 1962.

9. Lees, L., "Laminar Heat Transfer Over Blunt-Nosed Bodies at Hypersonic Flight Speeds," Jet Propulsion Lab, April, 1956.

10. Walker, G.K., "Some Comments on Laminar and Turbulent Heat Transfer Equations," GE RSD AETM 147, December, 1959.

11. Ekert, E.R.G., "Engineering Relationships for Heat Transfer and Friction in High Velocity Laminar and Turbulent Boundary Layer Flow over Surfaces with Constant Pressure and Temperature," ASME Paper No. 55-A-31, 1955.

12. Walker, G.K., "Turbulent Boundary Correction at High Reynolds Numbers," GE RSD TFM-8151-006, November 2, 1962.

13. Berman, R.J., "A Method for Prediction of Bow Shock Wave about Sphere Cones," GE RSD AFM 127, 1961.

14. Sutherland, W., Phil. Mag., Vol. 5, No. 36, p 507, 1863.

15. National Bureau of Standards Circular, No. 564, November 1, 1955.

REFERENCES (Continued)

16. Logan, J.G., and Treanor, C.E., "Tables of Thermodynamic Properties of Air," Cornell Aeronautical Laboratory Report BE-1007-A-3, January, 1957.

17. Munson, T. and Spindler, R., "Transient Thermal Behavior of Decomposing Materials, Part I; General Theory and Application to Convective Heating," paper presented at IAS 30th Annual Meeting, New York, New York, January, 1962.

18. Gordon, P., "Analysis of One-Dimensional Heat Conduction Computer Program," GE TIS R66SD10, March, 1966.

DOCUMENT CONTROL DATA - R&D

(Security classification of title, body of abstract and indexing annotation must be entered when the overall report is classified)

1 ORIGINATING ACTIVITY (Corporate author)	2a REPORT SECURITY CLASSIFICATION
General Electric Company	Unclassified
Re-entry and Environmental Systems Division	2b GROUP
Philadelphia, Pa.	

3 REPORT TITLE

DEVELOPMENT OF A FLEXIBLE ABLATOR FOR EXPANDABLE RE-ENTRY BODIES

4 DESCRIPTIVE NOTES (Type of report and inclusive dates)

Summary Technical Report, April 15, 1969 to July 31, 1969

5 AUTHOR(S) (Last name, first name, initial)

A. L. Levine	D. E. Florence	R. Gluck
R. C. Thuss	D. Lowe	J. Kohr

6 REPORT DATE	7a TOTAL NO. OF PAGES	7b NO OF REFS
April 14, 1970	—	18

8a CONTRACT OR GRANT NO	9a ORIGINATOR'S REPORT NUMBER(S)
F 33615-69-C-1713	69SD921
b PROJECT NO	
8170	
c	9b OTHER REPORT NO(S) (Any other numbers that may be assigned this report)
d	AFAPL-TR-70-15

10 AVAILABILITY/LIMITATION NOTICES

Each transmittal of this document outside the Department of Defense must have prior approval of the Air Force Aero Propulsion Laboratory, Wright Patterson Air Force Base, Ohio, 45433.

11 SUPPLEMENTARY NOTES	12 SPONSORING MILITARY ACTIVITY
	Air Force Aero Propulsion Laboratory
	Wright Patterson Air Force Base, Ohio 45433

13 ABSTRACT

The Phase I investigation to evaluate and select a flexible ablator material for expandable re-entry bodies was completed. All materials under consideration were compatible with the thermal environment. Thermal shield selection was based on results of a foldability rating index established on the basis of material mechanical properties.

The thermal shield system selected for further study is a composite elastomeric system consisting of a GE Blue overlay on ESM 1030.

DD FORM 1473 JAN 64

14 KEY WORDS	LINK A		LINK B		LINK C	
	ROLE	WT	ROLE	WT	ROLE	WT
Flexible						
Ablator						
Re-entry						
Expandable						
Vehicle						

INSTRUCTIONS

1. ORIGINATING ACTIVITY: Enter the name and address of the contractor, subcontractor, grantee, Department of Defense activity or other organization (*corporate author*) issuing the report.

2a. REPORT SECURITY CLASSIFICATION: Enter the overall security classification of the report. Indicate whether "Restricted Data" is included. Marking is to be in accordance with appropriate security regulations.

2b. GROUP: Automatic downgrading is specified in DoD Directive 5200.10 and Armed Forces Industrial Manual. Enter the group number. Also, when applicable, show that optional markings have been used for Group 3 and Group 4 as authorized.

3. REPORT TITLE: Enter the complete report title in all capital letters. Titles in all cases should be unclassified. If a meaningful title cannot be selected without classification, show title classification in all capitals in parenthesis immediately following the title.

4. DESCRIPTIVE NOTES: If appropriate, enter the type of report, e.g., interim, progress, summary, annual, or final. Give the inclusive dates when a specific reporting period is covered.

5. AUTHOR(S): Enter the name(s) of author(s) as shown on or in the report. Enter last name, first name, middle initial. If military, show rank and branch of service. The name of the principal author is an absolute minimum requirement.

6. REPORT DATE: Enter the date of the report as day, month, year; or month, year. If more than one date appears on the report, use date of publication.

7a. TOTAL NUMBER OF PAGES: The total page count should follow normal pagination procedures, i.e., enter the number of pages containing information.

7b. NUMBER OF REFERENCES: Enter the total number of references cited in the report.

8a. CONTRACT OR GRANT NUMBER: If appropriate, enter the applicable number of the contract or grant under which the report was written.

8b, 8c, & 8d. PROJECT NUMBER: Enter the appropriate military department identification, such as project number, subproject number, system numbers, task number, etc.

9a. ORIGINATOR'S REPORT NUMBER(S): Enter the official report number by which the document will be identified and controlled by the originating activity. This number must be unique to this report.

9b. OTHER REPORT NUMBER(S): If the report has been assigned any other report numbers (*either by the originator or by the sponsor*), also enter this number(s).

10. AVAILABILITY/LIMITATION NOTICES: Enter any limitations on further dissemination of the report, other than those imposed by security classification, using standard statements such as:

  (1) "Qualified requesters may obtain copies of this report from DDC."

  (2) "Foreign announcement and dissemination of this report by DDC is not authorized."

  (3) "U. S. Government agencies may obtain copies of this report directly from DDC. Other qualified DDC users shall request through

    _____ ."

  (4) "U. S. military agencies may obtain copies of this report directly from DDC. Other qualified users shall request through

    _____ ."

  (5) "All distribution of this report is controlled. Qualified DDC users shall request through

    _____ ."

If the report has been furnished to the Office of Technical Services, Department of Commerce, for sale to the public, indicate this fact and enter the price, if known.

11. SUPPLEMENTARY NOTES: Use for additional explanatory notes.

12. SPONSORING MILITARY ACTIVITY: Enter the name of the departmental project office or laboratory sponsoring (*paying for*) the research and development. Include address.

13. ABSTRACT: Enter an abstract giving a brief and factual summary of the document indicative of the report, even though it may also appear elsewhere in the body of the technical report. If additional space is required, a continuation sheet shall be attached.

It is highly desirable that the abstract of classified reports be unclassified. Each paragraph of the abstract shall end with an indication of the military security classification of the information in the paragraph, represented as *(TS), (S), (C),* or *(U)*.

There is no limitation on the length of the abstract. However, the suggested length is from 150 to 225 words.

14. KEY WORDS: Key words are technically meaningful terms or short phrases that characterize a report and may be used as index entries for cataloging the report. Key words must be selected so that no security classification is required. Identifiers, such as equipment model designation, trade name, military project code name, geographic location, may be used as key words but will be followed by an indication of technical context. The assignment of links, rules, and weights is optional.